Dalton Transactions

ROYAL SOCIETY OF CHEMISTRY

PAPER

View Article Online
View Journal | View Issue

Check for updates

Cite this: *Dalton Trans.*, 2020, **49**, 2862

Metal self-assembly mimosine peptides with enhanced antimicrobial activity: towards a new generation of multitasking chelating agents†

Joanna Izabela Lachowicz, *[a] Gabriele Dalla Torre, [b,c] Rosita Cappai,[d] Enrico Randaccio,[e] Valeria M. Nurchi, [d] Remigiusz Bachor,[e] Zbigniew Szewczuk, [e] Lukasz Jaremko,[f] Mariusz Jaremko, [f] Maria Barbara Pisano,[g] Sofia Cosentino,[g] Germano Orrù,[h] Antonella Ibba,[h] Joni Mujika[b] and Xabier Lopez*[b]

Mimosine is a non-protein amino acid with various properties, such as antibacterial, anti-inflammatory, anti-cancer and anti-virus among others. Due to its structural similarity with deferiprone (**DFP**), mimosine is a potential excellent metal chelator. In the present work, we combine experimental and theoretical (DFT) approaches in order to investigate the properties of mimosine peptides. Six different peptides were synthesized and their complex stoichiometry and stability were characterized by means of UV-Vis spectrophotometry. Then, the binding mode and self-assembly features of the peptides were evaluated using a DFT approach, taking into account different number of mimosine amino acids and varying the length of the spacer between the mimosine residues, and there was good agreement between experimental data and computational calculations. Further elucidations of the structural properties of these peptides allowed us to propose improvements in the structure of the mimosine moiety which can lead to enhanced affinity for high-valent metals. Moreover, we demonstrate that these peptides show an antimicrobial activity against Gram positive bacteria that is enhanced by the formation of a complex with iron(III) ions. The mimosine peptides could be an alternative to antimicrobial peptides (AMPs), which are expensive and susceptible to proteolytic degradation. In summary, in the present work, we propose a new generation of multipurpose mimosine-based peptides as new metal self-assembly chelators which could be a turning point in biomedical and nanotechnological applications.

Received 26th November 2019,
Accepted 27th January 2020

DOI: 10.1039/c9dt04545g

rsc.li/dalton

1. Introduction

One out of three proteins use metal ions as cofactors. The binding of metal ions to proteins changes their structures and properties, and it is a key feature for their structural, regulatory, and/or enzymatic functions. For example, peptides that self-assemble through metal–ligand complexes form nanostructures that possess very different structures and functions from the original peptides. This particular property was recently used for the synthesis of metal-triggered, self-assembled peptides in nanotechnology,[1] to synthesize nanofiber materials for cell culture and tissue engineering,[2] to assemble peptide nanotubes[3] and helical ribbons, *etc.* Thus, the formation of molecular building blocks that can spontaneously form regular and stable macroscopic structures, *via* covalent or noncovalent bonds is a very active and fast-growing process in nanotechnology.

In addition to the 22 amino-acids used by eukaryotes, there are more than 140 non-proteinogenic amino-acids that are not

[a]*Department of Medical Sciences and Public Health, University of Cagliari, Cittadella Universitaria, 09042 Monserrato, Italy. E-mail: lachowicz@unica.it*
[b]*Kimika Fakultatea, Euskal Herriko Unibertsitatea UPV/EHU, Donostia International Physics Center (DIPC), P.K. 1072, Donostia, Euskadi, 20080 San Sebastian, Spain. E-mail: xabier.lopez@ehu.es*
[c]*UCIBIO/REQUIMTE, Departamento de Química e Bioquímica, Faculdade de Ciências, Universidade do Porto, Rua do Campo Alegre, s/n, 4169-007 Porto, Portugal*
[d]*Department of Life Sciences, University of Cagliari, Cittadella Universitaria, 09042 Monserrato, Italy*
[e]*Faculty of Chemistry, University of Wrocław, F. Joliot-Curie 14, 50-383 Wrocław, Poland*
[f]*Division of Biological and Environmental Sciences and Engineering, King Abdullah University of Science and Technology (KAUST), 23955 Thuwal, Saudi Arabia*
[g]*Department of Medical Sciences and Public Health, University of Cagliari, Cittadella Universitaria, 09042 Monserrato, Italy*
[h]*Department of Surgical Sciences, University of Cagliari, Cittadella Universitaria, 09042 Monserrato, Italy*

†Electronic supplementary information (ESI) available. See DOI: 10.1039/C9DT04545G

naturally encoded or found in the genetic code of any organism. Some of them possess a biological function (*e.g.* components of bacterial cell walls, neurotransmitters and toxins) that may be used as natural or man-made pharmacological compounds.[4]

Antibiotics are among the most extensively used drugs. Their abuse in human medicine and in animal farming leads to bacteria resistance.[5] Now, we are witnessing the end of a golden epoch of antibiotics[6] and new solutions are critical for human health. Antimicrobial peptides (AMPs) have emerged as an alternative to antibiotics and in 2003 Daptomycin (MIC 32 μg ml^{-1} (ref. 7)) was approved by the FDA as an antibiotic against a variety of Gram-positive bacteria (methicillin-resistant *Staphylococcus aureus* (MRSA), vancomycin-resistant *enterococci* (VRE) and penicillin-resistant *Streptococcus pneumoniae*[8] (PRSP)). The bactericidal activity of AMPs is triggered mainly by membrane disruption and reduction in bacterial resistance; however most AMPs are expensive, highly cytotoxic and susceptible to proteolytic degradation. AMPs can be improved by the design of peptide mimics (peptidomimetics), whose backbone is not based on the regular amino acid linked in a chain.[9,10] One of the strategies in peptidomimetics is the use of unnatural amino acids.[11]

Mimosine [β-[*N*-(3-hydroxy-4-oxypyridyl)]-α-aminopropionic acid] (**MIM**, Scheme 1) is a non-protein amino-acid biosynthesized by the *Mimosoideae* family of plants. The chemistry,[12] methods for estimation,[13] biosynthesis,[14] and the degradation of this secondary metabolite[15] have been extensively described in the literature. Over the past few years, mimosine has been found to be involved in different biological processes such as

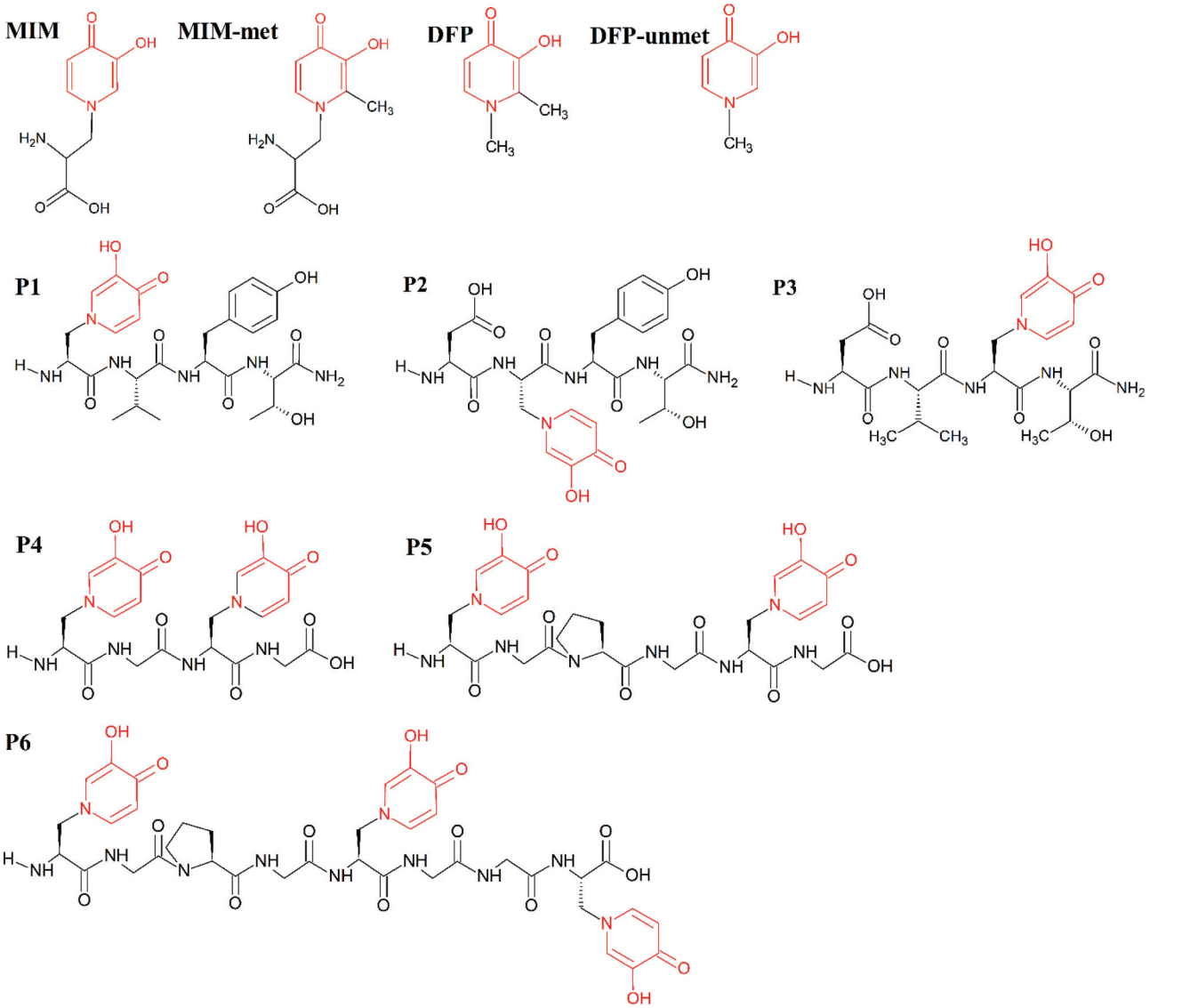

Scheme 1 Molecular structures of the studied molecules (**MIM**, **MIM-unmet**, **DFP**, **DFP-unmet**, **P1–P6**). Structural similarities between these molecules are indicated in red.

antibacterial,[16] anti-cancer,[17] anti-inflammatory,[18] anti-fibrosis,[19] anti-influenza,[20] anti-virus,[21] herbicidal[22] and insecticidal,[23] among others.[12] In the 90s, mimosine was investigated as a potential inhibitor of the G1/S phase,[24] and, over the last twenty years, as a potential drug for cancer.[25] The activity of mimosine-based peptides has been linked to its metal chelating properties. For instance, the coordination of the essential metal ions, in blood plasma, causes an inhibition of the growth of wool and defleecing in sheeps.[26]

The mimosine sidechain is structurally similar to that of deferiprone (**DFP**, Ferriprox, 1,2-dimethyl-3-hydroxy-4-pyridinone, Scheme 1) and therefore, they show similar features in their metal-coordination ability. **DFP** is used as a drug to remove the excess iron in thalassaemia major.[27] It has been used in the treatment of thalassaemia major in Europe and Asia since 1994, and was approved for its use in the US,[28] in 2011. Its coordination of Cu(II),[29,30] Cd(II),[31] Al(III),[32] Fe(III),[33] Ga(III),[34] Gd(III),[29] and In(III)[34] metal ions, as well as actinides[35] and lanthanides,[36] has been extensively described in the literature. **DFP** and its derivatives have been proposed as potential remedies for diseases related to metal disorders, *e.g.* anaemia, thalassemia, hemochromatosis, *etc.*, for which the delivery, or removal, of metal ions is desirable. Recently, hydroxypyridinones have been used to improve the retention and tissue uptake of metal-based insulin-enhancing agents. **DFP**-based therapy protects against the toxicity of heavy metals (used in contrast agents), chemotherapeutics, exposition to harmful radioisotopes and the neurotoxicity of redox metals.[37] Fe(III)–, VO(IV)–, Cu(II)–, Zn(II)– and Ni(II)–mimosine complexes have been investigated by various research groups.[38,39] Mimosine dipeptides and tetrapeptides have been previously synthesized and investigated as potential neuraminidase,[40] tyrosinase[40,41] and cyclooxigenase[41] inhibitors. However, to our knowledge, no other applications have been considered, nor any synthesis of mimosine hexapeptides has been performed, to this day.

Recently, we have investigated by means of QM/MM and DFT calculations the potential application of several mimosine-based peptides as improved metal chelators.[42] We found that this class of ligands may reach a metal binding affinity comparable to or even higher than **DFP**.[42] In this paper, we present synthetic, DFT, and experimental iron(III)- and copper (II)-complex formation studies of tetra- and hexapeptides containing one, two or three mimosine residues. The antimicrobial activities of the synthesized complexes against Gram positive, Gram negative bacteria and dermatophytes are also investigated and reported here (Section 3.2). We found very good agreement between experimental and theoretical studies, which point to these mimosine-based peptides as effective iron(III) and copper(II) chelators. The effect on the affinity of key structural features of these peptides, such as the number of mimosine residues and length and flexibility of the spacer, is also discussed and rationalized. The DFT model established here can be used for the design of the self-assembly of metal ions and mimosine peptides for medical and nanotechnological applications.

2. Experimental

2.1. Reagents

All solvents and reagents were used as supplied. Fmoc amino acid derivatives were purchased from Novabiochem. $FeCl_3$, $CuCl_2 \times 2H_2O$, NaOH, HCl, L-mimosine was obtained from Sigma Aldrich. (Benzotriazol-1-yloxy)tris(pyrrolidino)phosphonium hexafluorophosphate (PyBOP), *N*-[(dimethylamino)(1*H*-1,2,3-triazolo-[4,5-*b*]pyridin-1-yl)methylene]-*N*-methylmethanaminium hexafluorophosphate *N*-oxide (HATU), and MBHA-Rink amide resin (0.69 mmol g^{-1}) were obtained from Merck Millipore. Fmoc-Gly-Wang resin (0.73 mmol g^{-1}), 2-chlorotrityl chloride resin (1.00 mmol g^{-1} and trifluoroacetic acid (TFA) were obtained from IrisBiotech. Solvents for peptide synthesis (*N*,*N*-dimethylformamide (DMF), dichloromethane (DCM), and (*N*-ethyldiisopropylamine (DIEA)) were obtained from Sigma Aldrich.

2.2. Synthesis

The synthesis of the Fmoc-Mim derivative was performed using the method described by Upadhyay *et al.*[40] Briefly, mimosine (200 mg) and sodium carbonate (Na_2CO_3) (220 mg) were dissolved in distilled water (3 mL). Fmoc-Osu (500 mg) dissolved in 3.6 mL of 1,4-dioxane was added dropwise to the solution and stirred for 2 h at room temperature. Afterwards, 12 mL of Na_2CO_3 (0.1 M) was added. The mixture was stirred for 7 h at 26 °C and was then filtered and washed with 20 mL of ethyl acetate to remove the excess of Fmoc-Osu and by-products. The water fraction was kept in an ice bath, the pH was adjusted to 4.0 (by adding 6 N HCl) and the mixture was incubated overnight at 4 °C. The resulting precipitate was filtered, washed with distilled water, and dried under reduced pressure to give Fmoc mimosine. The obtained product was analyzed by ESI-MS.

The synthesis of peptides on the MBHA-Rink (peptides 1–3, Table S1†), Fmoc-Gly-Wang resin (peptide 4, Table S1†) and 2-chlorotrityl chloride resin was performed manually in polypropylene syringe reactors (intavis AG) equipped with polyethylene filters, according to a standard Fmoc (9-fluorenylmethoxycarbonyl) solid phase synthesis procedure.[43]

All products were purified using the analytical HPLC Thermo Separation system with UV detection (210 nm) having a YMAC-Pack RP C18 Column (4.6 × 250 mm, 5 μm), with a gradient elution of 0–40% *B* in *A* (*A* = 0.1% TFA in water; *B* = 0.1% TFA in acetonitrile/H_2O, 4 : 1) over 30 min (flow rate 1 mL min^{-1}). The main fraction, corresponding to the peptide, was collected and lyophilized.

All products were analyzed on a microTOF-Q mass spectrometer (Bruker Daltonics, Bremen, Germany) and on an FTICR (Fourier Transform Ion Cyclotron Resonance) PAex-Qe Ultra 7 T mass spectrometer (Bruker Daltonics, Bremen, Germany) equipped with a standard ESI source. The instruments were operated in the positive-ion mode and calibrated daily with a Tunemix™ mixture (Agilent Technologies, Palo Alto, CA, USA). The mass accuracy was better than 5 ppm. Analyte solutions (70 μl) were introduced at a flow rate of 3 μl min^{-1}. The parameters of the instruments were as follows: for microTOF-Q

Table 1 Constants of formation for the Iron(III)–**DFP** and Iron(III)–mimosine Systems, as determined at t = 25 °C and I = 0.1 M (KCl) by Nurchi,[32] and at t = 25 °C and I = 0.1 M Tsai and Ling,[58] respectively. Stability constants of the proton and Cu(II) complexes of **DFP** at t = 37 °C and I = 0.15 (KNO_3) by Stunzi *et al.*,[59] and at t = 25 °C and I = 0.1 M (KCl) by Nurchi *et al.*;[32] L-mimosine, t = 37 °C and I = 0.15 (KNO_3) by Stunzi *et al.*[59] and at t = 25 °C and I = 0.1 M (KNO_3) by Chruscinska *et al.*[38]

	DFP[32]			Mimosine[58]		**DFP**[59]	**DFP**[32]	Mimosine[59]			Mimosine[38]
Species	log K			log K	Species	log K	log K	log K			log K
LH	9.82			8.76	LH	8.80	9.82	8.86			9.02
LH_2	3.66			7.14	LH_2	3.35	3.66	7.00			7.18
LH_3				2.48	LH_3	—	—	2.62			2.56
					LH_4	—	—	1.1			<1
Species	log K	λ_{max}	ε	log K	Species	log K	log β	log β	λ_{max}	ε	log β
					$CuLH_2$			18.1			
FeLH				12.00	CuLH	1.60		16.36	755	34 ± 5	16.63
FeL	15.01	540	1700		CuL	9.35	10.42	9.48			
					$CuLH_{-2}$						−9.47
FeL_2H_2				9.50	CuL_2H_2	—		31.26	693 ± 10	37 ± 10	32.04
					CuL_2H		21.98	24.40			24.43
FeL_2	12.02	491	3700		CuL_2	7.58	19.09	16.81	690	33	17.23
					CuL_2H_{-1}		8.49				5.79
					Cu_2L			15.70	735 ± 15	28 ± 5	
					Cu_2L_2			32.2	662	50	29.98
					Cu_2L_3			29.52			
FeL_3H_3				8.00							
FeL_3H_2				6.28							
FeL_3H				7.43							
FeL_3	10.40	457	4400	7.42							

MS: scan range: 50–1600 m/z; drying gas: nitrogen; flow rate: 4.0 L min^{-1}, temperature: 200 °C; potential between the spray needle and the orifice: 4.2 kV; for FTICR MS: scan range: 100–1600 m/z; drying gas: nitrogen; flow rate: 1.5 L min^{-1}, temperature: 200 °C; potential between the spray needle and the orifice: 4.2 kV. For MS spectra analysis (Table 1), a Bruker Compass Data Analysis 4.0 software was used.

2.3. NMR measurements

2.0 mg of each peptide was dissolved in 500 μL of a mixture of 10% D_2O and 90% of H_2O (v/v). After the peptide was dissolved, the pH of the solution was manually adjusted to 7.40, prior to each measurement. All NMR experiments were performed using either 700 MHz (for peptides 1 and 2) or 950 MHz (for peptides 3–5) spectrometers at 25 °C. All NMR data were processed by NMRPipe[44] and analyzed by using Sparky[45] software. Complete assignments of the ^1H and ^{13}C resonances, for all the peptides (Tables S3–S7†), were done by the application of a standard procedure[46] based on the inspection of the 2D homonuclear TOCSY (with mixing times of 10 and 80 ms) and ROESY (with mixing times of 300) experiments. The NMR spectra were acquired after 2 months of synthesis and ESI-MS spectra acquisition. No peptide degradation was observed.

2.4. UV-Vis measurements

UV-Vis spectra were recorded using a SPECTROstar Nano (BMG LABTECH). 5 μl total volume of the peptide and metal water solutions were placed in multi-well plates, and spectra were collected, using a range of wavelengths from 200 to 900 nm. The final pH was a result of mixing peptide- and water solutions with metal acidic solutions. The peptide and metal concentrations, for each experiment, are reported in the Results and Discussion section. The pHs of the solutions were measured using a METROHM Microelectrode 6.0224.100 daily calibrated with a Mettler TOLEDO InLab® Solutions buffer (pHs 4.01 and 9.21).

2.5. ESI-MS measurements

The obtained mass spectra were recorded in the positive mode on a LCMS 9030 qTOF Shimadzu mass spectrometer (Shimadzu, Kyoto, Japan). The m/z range was between 100 and 1500, interface voltage (+) was 4.5 kV, interface temperature 300 °C, DL temperature 250 °C, heat block temperature 400 °C, nebulizing gas (nitrogen) flow 3 L min^{-1}, and total flow 0.4 mL min^{-1} of the H_2O/MeCN mixture (1 : 1, v : v). Equimolar ratios of the peptide and metal ions (Fe(III) ions ($FeCl_3$), Cu(II) ($CuSO_4$) were mixed in water, dissolved in methanol and analyzed by mass spectrometry.

2.6. DFT calculations

Optimization was carried out using the B3LYP functional[47,48] with Grimme's D3 dispersion correction[49] along with the Becke–Johnson (BJ) damping scheme and the 6-31+G(d) basis set. To confirm that the optimized structures were real minima on the potential energy surfaces, frequency calculations were carried out at the same level of theory. All structures showed positive force constants for all normal modes of vibration. The frequencies were then used to evaluate the zero-point vibrational energy (ZPVE) and thermal (T = 298°K) vibrational corrections to the Gibbs free energies within the harmonic oscillator approximation. To calculate the entropy, the

different contributions to the partition function were evaluated using the standard statistical mechanics expressions in the canonical ensemble and the harmonic oscillator and rigid rotor approximation. In addition, energies were refined with single point calculations at the B3LYP-D3(BJ)/6-311++G(3df,2p) level of theory. All calculations were performed with the IEFPCM solvation model[50] in order to properly investigate the thermodynamics of metal–ligand complexes in solution.

All calculations were performed with the Gaussian16 Rev. A03 package.[51]

Binding energies and enthalpies were calculated according to the following substitution reaction:

$$\begin{aligned}&\left[M(H_2O)_6\right]^p + n[LIG]^q \\ &\quad \leftrightarrow \left[M(H_2O)_{6-m}(LIG)_n\right]^{p-nq} + m(H_2O)\end{aligned} \tag{1}$$

where M can be Fe(III)(sextuplet) or Cu(II)(doublet), p refers to the metal charge (+3 for Fe(III) and +2 for Cu(II)), LIG is one of the ligands (**DFT**, **DFT-unmet**, **MIM**, **MIM-unmet**, peptides 1–6) depicted in Scheme 1, n refers to the number of the ligand (n = 1,2,3), q is the total charge of the ligand, and m is the number of water molecules displaced from $M(H_2O)_6$ by the n ligands so that $m = 2n$ (note that every ligand binds bidentately to the metal).

Ligands were considered in their unprotonated form since this is the way that experimental stability constants are calculated, and good agreement was found between DFT binding energies and experimental $\log\beta$ values as in a previous work.[52]

The binding energies in solution associated with eqn (1) can be calculated as:

$$\begin{aligned}\Delta G_{aq}^{comp} = {} & G_{aq}\left[M\cdot(H_2O)_6 - m(LIG)^n\right] + mG_{aq}(H_2O) \\ & - G_{aq}\left[M(H_2O)_6\right] - nG_{aq}(LIG) \\ & + \Delta vRT\ln(24.46) + mRT\ln(55.34)\end{aligned} \tag{2}$$

Since the energies were determined using an ideal gas at 1 atm as the standard state, the penultimate term in eqn (2) corresponds to the volume change due to the transformation from 1 atm to 1 M in solution, where Δv refers to the change in the number of species in the reaction. The last term is the entropic factor that accounts for the concentration of 55.34 M of water in liquid water.[53] The $\Delta vRT\ln(24.46)$ and $mRT\ln(55.34)$ corrections correspond to the changes in the standard state, accounting, on the one hand, for the change due to the transformation from 1 atm to 1 M in solution, and to an entropic factor that accounts, on the other hand, for the concentration of 55.34 M of water in liquid.[53]

2.7. Antimicrobial activity

2.7.1. Bacterial and dermatophyte species and culture conditions. The antibacterial and antifungal activities of the six peptides were preliminarily evaluated by the agar-plate disk-diffusion method (CLSI) against the following bacterial and dermatophyte species: *Staphylococcus aureus* ATCC 25923, *Bacillus cereus* ATCC 11178, *Escherichia coli* ATCC 25922, *Microsporum canis* 10D, and *Trichophyton rubrum* 11D (from the collection of the Department of Medical Science and Public Health). All bacterial strains were stored in a nutrient broth (NB, Microbiol, Cagliari, Italy) and 15% (v/v) glycerol, at −20 °C, except the dermatophyte strains that were maintained in Potato Dextrose broth (PDB, Microbiol) with 15% (v/v) glycerol. Before use, they were sub-cultured twice in an appropriate medium.

The bacterial and fungal suspensions, adjusted to a 0.5 McFarland standard turbidity (equivalent to 1.5×10^8 CFU mL^{-1} or 1–5 × 10^6 spores per mL^{-1}),[54] were prepared in NB and in sterile phosphate-buffered saline (PBS) with 0.05% Tween 80 (PBS-Tween), respectively.

A sterilized filter paper disc (5 mm in diameter) containing either a 10 μL of peptide or a Cu(II)–peptide complex sample was placed on Muller Hinton (MHA) or Sabouraud Dextrose agar (SDA) plates previously seeded with the prepared bacterial and fungal suspensions. Different stock solutions of peptides were prepared, depending on the residual amount. Peptides 1, 3 and 5 were dissolved in 0.2 mL of sterile distilled water to obtain the final concentrations of 50, 340, and 810 μg per disc, respectively. Peptides 2 and 4 were dissolved in 0.5 mL of sterile distilled water to obtain 84 and 149 μg per disc concentrations, respectively. The stock solution of peptide 6 prepared in DMSO (100%) was further diluted in NB to obtain the final concentrations of 140 and 14 μg per disc. These concentrations were chosen according to each peptide maximum-water solubility. The Cu(II)–peptide complexes involving peptides 2, 4 and 6 were prepared in 1 : 3, 1 : 1 and 1 : 1 metal-to-peptide molar ratios, respectively. 25 μg of amoxicillin, 5 μg of ofloxacin or 15 μg of Ketoconazole (Oxoid) and blank disc impregnated with 10 μL of NB or PBS-Tween were used as positive and negative controls, respectively.

Serial doubling dilutions of the different peptides and their metal complexes were prepared in 100 μL of NB, in 96-well microtiter plates. The following concentrations were tested: **P3**, 3400–106.25 μg mL^{-1}, **P4**, 7450–232.81 μg mL^{-1}, **P5**, 8100–253.125 μg mL^{-1}, **P6**, 6900–215.625 μg mL^{-1}, for the following metal–peptide complexes: Fe(III)–**P1** 333.7–3.0 μg mL^{-1}, Fe(III)–**P2** (1 : 3 metal : peptide molar ratio) 560–17.5 μg mL^{-1}, Fe(III)–**P4** (1 : 1 metal : peptide molar ratio) 967.5–30.2 μg mL^{-1}, Fe(III)–**P6** (1 : 1 metal : peptide molar ratio) 896.1–28.0 μg mL^{-1}. The bacterial suspensions, prepared as described above, were further diluted in the broth media, and 100 μL volume of this diluted inoculum was added to each well of the plate, resulting in the final inoculum of 5×10^5 CFU mL^{-1}. Controls for the sterility of the NB and the peptides, and the culture (inoculum) were included; DMSO (for **P6**) was also monitored to check the effect of the solvent on the growth of microorganisms. Furthermore, ofloxacin (8 μg mL^{-1}) was used as the positive control for Gram-positive and negative bacteria. MICs and MBCs were determined after 24 h of incubation of the plates, at 37 °C. Microbial growth was indicated by the presence of turbidity and a "pellet" on the well bottom. MICs were determined presumptively as the first well, in ascending order, which did not produce a pellet. To confirm MICs and to establish MBCs, 10 μL of broth was removed from each well and

inoculated on Tryptic Soy Agar (Microbiol) plates. After incubation under the conditions described above, the number of surviving bacteria was determined. The MIC was the lowest concentration that resulted in a significant decrease of the inoculum's viability (>90%), and the MBC concentration was found to be the one for which 99.9% (or more) of the initial inoculum was killed. All tests were conducted in triplicate, and the modal MIC and MBC values were selected.

The MIC dilutions were prepared with daily prepared solutions and with 2 month-old solutions (stored at −5 °C). No differences were observed in the experimental results.

2.7.2. Antibiofilm activity. The following bacterial species were used: *Staphylococcus aureus* ATCC 6538 (American Type Culture Collection), *Streptococcus intermedius* DSMZ 20573 (German Collections of Microorganisms and Cell Cultures), *Pseudomonas aeruginosa*, strain ATCC 2783. These strains were cultured at 37 °C in the following: Mueller-Hinton broth for *S. aureus* and *P. aeruginosa*, and Schaedler broth for *S. intermedius*. All media were manufactured by Microbiol (Uta, Italy). The crystal violet staining protocol, previously described in the literature,[55] was used for biofilm evaluation. A microplate containing serial concentrations of the compound, inoculated with 10^6 CFU ml^{-1} bacterial cells, was incubated at 37 °C for 6 days, to permit biofilm formation. The plate samples were subsequently washed three times with phosphate-buffered saline GIBCO® PBS (ThermoFisher) to eliminate planktonic cells; thus the biofilm was stained with 100 μL of 0.1% w/v of crystal violet solution (Microbial, Uta, Italy) for 10 min at 25 °C; after washing with PBS solution three times, 200 μL of 30% v/v acetic acid was added in every well to solubilize the dye from the bacterial biomass. The biofilm amount was measured with a plate reader spectrophotometer (SLT-Spectra II, SLT Instruments, Germany) at 620 nm. For each formulation the experiment was performed in triplicate. For the same concentration, all values that showed a standard deviation (SD) within ±10% of the mean value were considered significant.

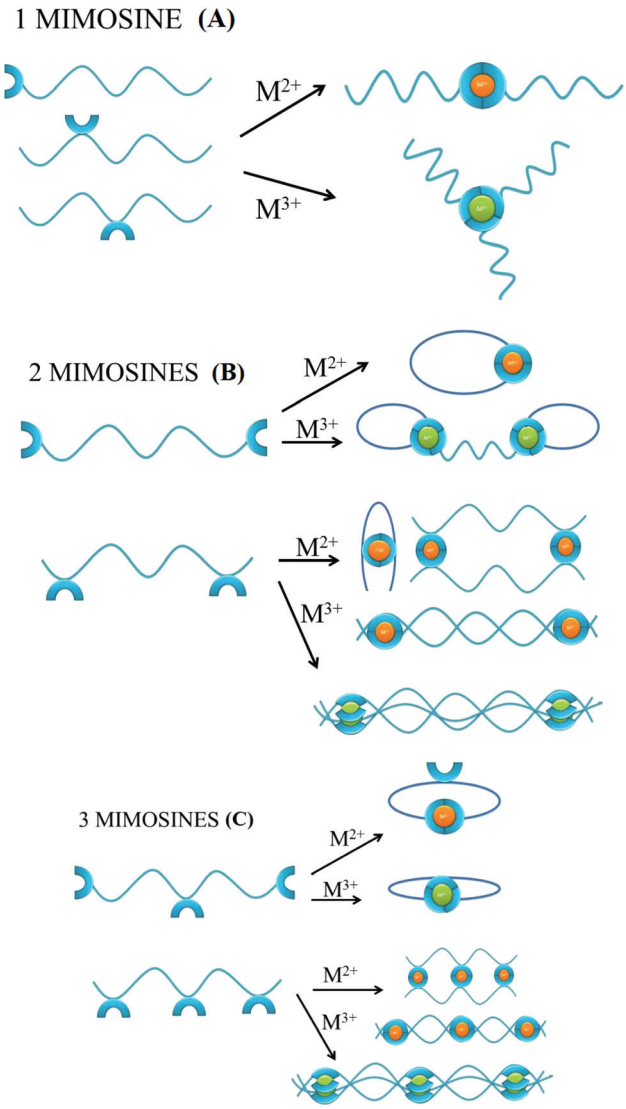

Scheme 2 Possible types of the self-assembled metal–peptide aggregates, according to the number of mimosine residues, the position of the mimosine in the backbone of the peptide, and the oxidation state of the metal.

3. Results and discussion

3.1. Metal coordination

The number of mimosine residues, their positions in the peptide backbone, and the length of the spacer between neighboring mimosine residues determine the stoichiometry of metal–peptide complexes and their structures (Scheme 2). Some of the predicted stoichiometries of the M^{2+} and M^{3+} metal-ion complexes with mimosine peptides are shown in Scheme 2, together with their possible structures.

In the peptide containing one mimosine residue (Scheme 2A), the most probable stoichiometry with M^{2+} is a 1 : 2 (metal : ligand) molar ratio, whereas in the trivalent metal ion, a 1 : 3 (metal : ligand) stoichiometry is expected. The position of the mimosine residue in the peptide backbone influences the ternary structure of the metal complex, and in some cases, where the conformational constraints occur, even the changes in the metal–ligand stoichiometry.

The addition of the second mimosine residue in the peptide backbone (Scheme 2B) gives more possible stoichiometries of the metal complex and makes the coordination system more complicated. The peptide that contains mimosine amino acids at the N- and C-ends of the peptide can form cyclic complexes with divalent metal ions, if the length of the linker between mimosine residues is long enough for obtaining appropriate geometry of the metal complex. In the case of the short spacer between neighboring mimosine residues (*e.g.* mimosine residues in the middle of the peptide backbone), it is likely that bend, dimeric or polymeric structures will be formed. For trivalent metal ions, the two mimosine peptides will form 2 : 3 (metal : ligand) complexes of different ternary

structures (closed or linear) or polymers, depending on the length of the linker between mimosine units.

The presence of a third mimosine residue (Scheme 2C) makes the predictability of the complex stoichiometry harder. Two mimosine residues at the N- and C-ends of the peptide, and one in the middle, will form cyclic complexes with trivalent metal ions, but also with divalent ones. In the last case, one mimosine residue will have free binding sites, which could be the starting point to form higher stoichiometric complexes. Three mimosine residues in close proximity in the backbone will lead to the formation of 3 : 2, 3 : 3 (metal : ligand) linear complexes or polymeric structures with divalent and trivalent metal ions.

The possible formation of polymeric structures by mimosine peptides is intriguing. The two mimosine peptides (Scheme 3A) can form with M^{2+} metal ions in linear polymers, while three mimosine peptides can be assembled both in linear and in non-linear polymers (Scheme 3B).

The formation of polymeric structures instead of dimeric complexes depends on the length of the linker between neighbouring mimosine residues, as well as linker rigidity (peptide bonds or proline residues) and steric incumbrances in the metal complex. Moreover, the metal and peptide concentrations in the solution, pH, ionic strength, and temperature determining polymerization/aggregation process[56] influence the polymerization/aggregation process, but they are not the object of the present studies.

In order to predict accurately the stoichiometry and the structure of the investigated complexes, we establish a DFT calculation protocol and probe peptides with a variable number of mimosine residues and different lengths of the linker.

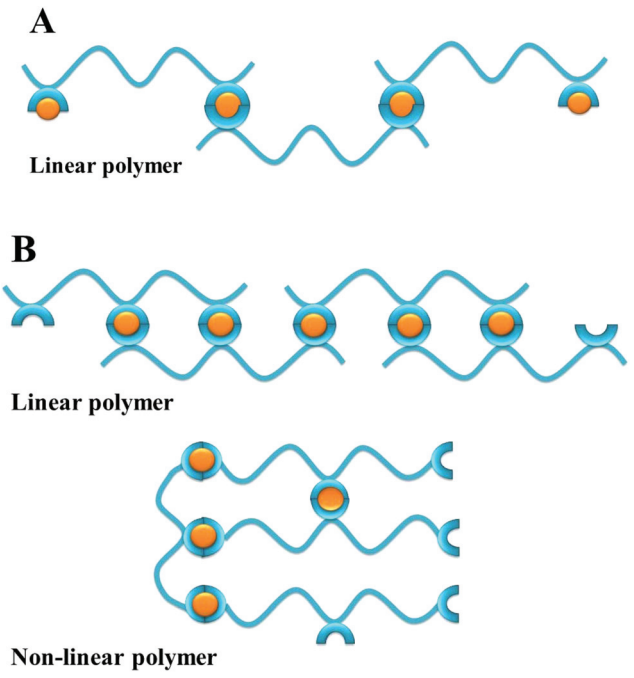

Scheme 3 Possible types of the self-assembled metal–peptide polymers with M^{2+}, according to the number of mimosine residues and the position of the mimosine in the backbone of the peptide.

3.1.1. DFP and mimosine Fe(III) and Cu(II) coordination models. The DFT protocol considers the metal coordination core, *i.e.* the hydroxypyridinone ring. As long as there are no crystal data for the mimosine complexes with copper(II) and iron(III) ions, the DFT model is prepared not only for **MIM** but also for **DFP**, which is the closest analogue of mimosine. The obtained data are then compared with the **DFP** crystal structure data.

The geometries of the 1 : 3 Fe(III)–ligand complexes with **MIM** and **DFP** show a perfect octahedral coordination mode (Fig. S1†), in agreement with the X-ray structure of the 1 : 3 Fe(**DFP**)$_3$ complex[34] (Fig. 1C). The octahedral geometry of the metal coordination shell is characterized by O–Fe–O angles between 80–90 and ~167 degrees, with the Fe–O distances 1.9–2.0 Å (Table S8†). Similarly, 1 : 2 and 1 : 1 Fe(III)–ligand complexes retain octahedral geometry with coordination sites filled by water molecules in the axial positions (Fig. S2 and S3†). On the other hand, in the 1 : 1 Cu(II)–ligand complex, one water molecule leaves the copper coordination sphere (Fig. S5†), and the system shows a pentacoordinate binding mode. In the 1 : 2 Cu(II)–ligand complex, two water molecules move away from their axial positions (Fig. S4†) and a stable tetrahedral complex is therefore formed, which is coherent with the X-ray structure for 1 : 2 Cu(II)–**DFP** (Fig. 1D).[57] The calculations with our DFT model are in line with experimental data (Table S2 and Fig. S8†).

In aqueous solution, **DFP** forms complexes with a 1 : 1 metal : ligand stoichiometry and at a pH lower than 1 (Fig. S6†) these complexes are transformed into 1 : 2 stoichiometry complexes above pH 2 and 1 : 3 complexes above pH 3.[32] The **DFP**–Fe(III) complexes are violet (at acidic pH) or red (neutral and basic pH), in water, and each complex is characterized by its specific absorptivity band (Fig. 1A). The crystal structure of **DFP** with Fe(III) ions (Fig. 1C) shows that the metal ion is coordinated in octahedral geometry by three pairs of carbonyl and dissociated hydroxyl groups.

With respect to L-mimosine, the protonation of the amino- and carboxylic groups makes the equilibrium of the iron complexation more complicated; nevertheless, electronic absorption spectra are similar to those obtained for **DFP** iron complexes, showing that amino- and carboxylic groups do not bind to the iron(III) ions.[39] The constants of formation for the **DFP** and **MIM** complexes with iron(III) ions, shown in Table 1, are in good correlation with the computed binding enthalpies (ΔH_{comp}) and free energies (ΔG_{comp}) for the complexes of similar stoichiometry, and with those calculated with our DFT model (Table S2 and Fig. S8†).

The aqueous solution complexes of **DFP** with copper(II) ions are green colored and the Vis spectra (Fig. 1B) in the 400–600 nm range show the charge transfer bands ($A_{max}\lambda$ ~ 480 nm) of O(phenol) to Cu(II) ions. Indeed, the crystal structure determined by A. El-Jammal *et al.*[57] (Fig. 1D) confirms the formation of a Cu(**DFP**)$_2$ complex and the coordination of copper ions by the pair of carbonyl and dissociated hydroxyl

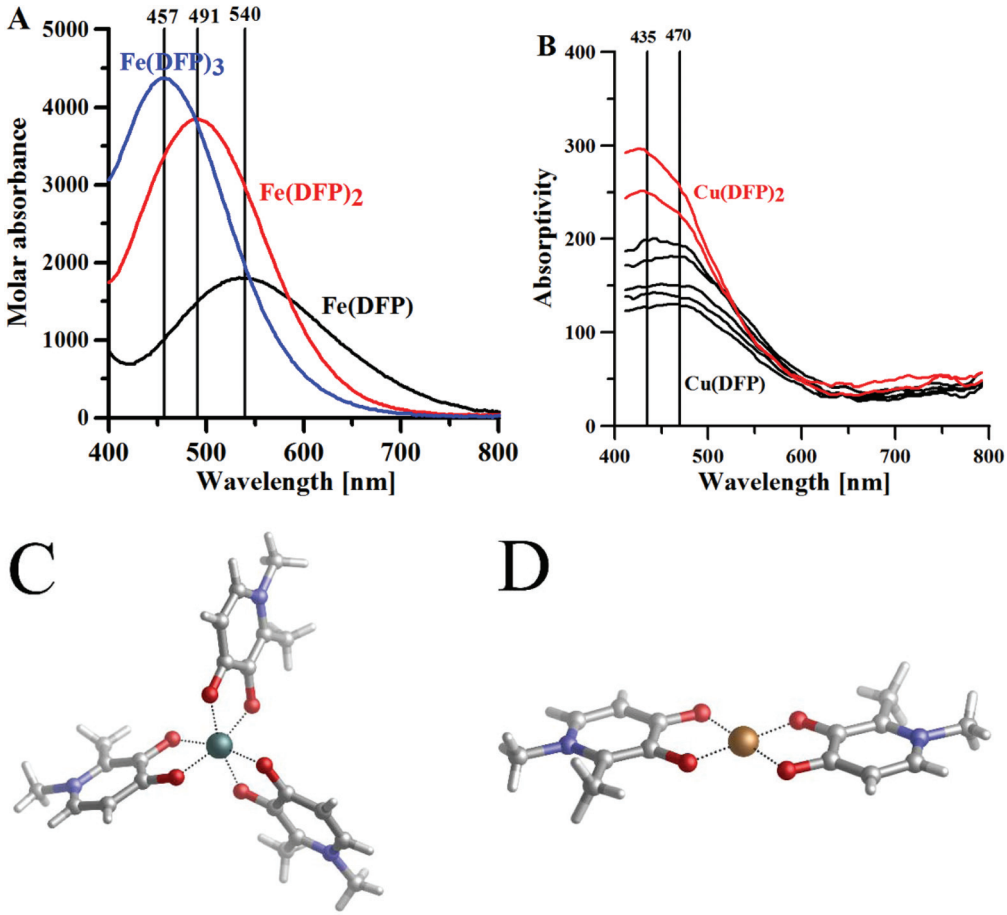

Fig. 1 The maximum absorptivity spectra of (A) Fe^{3+}–**DFP** complexes, [**DFP**] = 0.5 mM, l = 1 cm; (B) Cu(II)–**DFP** complexes, metal : ligand molar ratio 1 : 2, [**DFP**] = 0.5 mM, l = 10 cm. (C) Crystal structure CCDC (JAWSEF01, additional database identifier JUHXEP, 1183333) of Fe(**DFP**)$_3$ complexes by E. T. Clarke *et al.*[31] (D) The crystal structure (CCDC: 1291877, WELTEM) of the Cu(**DFP**)$_2$ complex by A. El-Jammal *et al.*[57]

groups in octahedral geometry, with two axial water ligands. As previously shown in the DFT calculations, the copper(II) complexes with **DFP** are less stable than the iron(III) complexes. The [Cu(**DFP**)]$^+$ forms at pH < 1 (Fig. S6†) and is replaced with the Cu(**DFP**)$_2$ complex above pH 2.5. The constants of stability of the copper(II)–**DFP** and mimosine complexes, presented in Table 1, are in good agreement with those calculated using our DFT model (Table S2†).

The copper(II)–**MIM** and copper(II)–**DFP** absorption spectra were studied by Stunzi *et al.*[59] According to the authors, the 1 : 1 (copper(II) : **MIM**) stoichiometry complexes have almost the same wavelength maxima (Table 1) as the corresponding **DFP** complexes. This finding confirms that the metal binding sites are similar for **MIM** and **DFP**. The addition of the spectra of CuDFP$^+$ and CuGly$^+$ (λ_{max} 715 nm)[60] reproduces approximately the spectrum of Cu$_2$(mimosine)$^{2+}$, whereas the spectrum of the dimeric 2 : 2 mimosine is similar to the mixed 1 : 1 : 1 Cu–Gly–**DFP** spectrum and has λ_{max} (660 nm) between those for the CuGly$_2$ (617 nm) and Cu(mimosine)$_2^{2-}$ (690 nm) complexes. The small extinction coefficient Cu$_2$(mimosine)$_2$ complex may be explained by a slightly distorted structure, essentially strain-free.

The formation of a dinuclear copper(II)–mimosine complex was confirmed by EPR studies, performed by Chruscinska *et al.*[38] A dinuclear species predominates in equimolar solution, for pHs ranging from pH 4 to 11 (Fig. S6†), and two sets of hyperfine components, each consisting of seven lines, at the approximate intensity ratio of 1 : 2 : 3 : 4 : 3 : 2 : 1, and in the parallel region of the $\Delta M_S = \pm 1$ resonances, are present in the EPR spectrum. The measured zero field splitting corresponds to an intermetallic distance of approximately 5.0 Å. The atoms from the donor sets are as follows: (CO, O$^-$) and (NH$_2$, COO$^-$).

Our DFT calculations confirm the stability of the dinuclear copper(II)–**MIM** complex. Fig. 2 shows the characteristics of the structure in which both Cu(II) cations are pentacoordinated by interacting with the backbone NH$_2$, the COO$^-$ groups of one **MIM**, and the carbonyl and hydroxyl oxygen atoms of the side chain of the other **MIM**. The metal coordination shell is completed by an explicit water molecule. The distances and angles computed (Table S10†) confirmed that the ligands are placed in a near-optimum arrangement. Compared to the Cu(**DFP**)$_2$ structure, the Cu–O distances in the dinuclear mimosine complex are slightly longer (1.94–1.97 Å) and the Cu–metal binding site angles are slightly different (90° and 170°) than

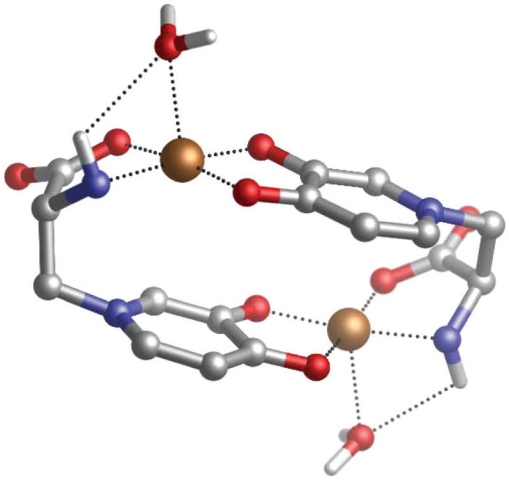

Fig. 2 DFT optimized structure of a dinuclear copper(II)–mimosine complex.

the corresponding distances (1.91–1.93 Å) and angles (90° and 180°) in the **DFP** copper complex (Table S10†). The DFT calculated distance between two copper ions in the dinuclear complex is 5.222 Å and stays in line with the EPR experimental data.[38] The stability of the complex was determined, *via* the following reaction:

$$2 \cdot \left[Cu(H_2O)_5\right]^{2+} + 2 \cdot [Mim]^{2-} \leftrightarrow \left[Cu_2 \cdot Mim_2 \cdot (H_2O)_2\right] + 8 \cdot (H_2O) \quad (3)$$

in which Cu(II) is always pentacoordinated. The computed value of the free energy of the complex (in triplet state) is −163.1 kcal mol^{-1} (ΔG_{aq}).

3.1.2. One-mimosine peptides: Peptide 1 (H-Mim-Val-Tyr-Thr-NH$_2$), Peptide 2 (H-Asp-Mim-Tyr-Thr-NH$_2$) and Peptide 3 (H-Asp-Val-Mim-Thr-NH$_2$). Here, we compare the metal complexes of four-amino acids peptides that contain only one **MIM** residue. According to the NMR data presented in Tables S3–S7,† none of the three peptides has a ternary structure. Peptide 1 contains one **MIM** residue at the N-end of the peptide, whereas peptide 2 and peptide 3 have **MIM** residues on the second and third positions, respectively.

The formation of metal complexes was studied experimentally using UV-Vis spectrometry, and the structure and stability of the formed complexes were determined by DFT calculations.

Electronic absorption spectra of the Peptide 1 (**P1**) and **P2** complexes with iron ions are shown in Fig. 3A. The **P1** peptide is considered to be a $[LH_3]^{2+}$ ligand, where the amine, amide and hydroxyl groups are the dissociating groups. In the solution containing iron(III) and **P1** at a molar ratio 1 : 1, and at pH 1.0, one band with a maximum absorptivity at 540 nm can be seen on the Vis spectrum, and it can be associated with the $[Fe(\mathbf{P1})H_2]^{4+}$ complex, as with the **DFP** complexes. The dissociated hydroxyl group is coordinating the iron ion, whereas both N-end and C-end (amide protected) of the peptide remain protonated, at pH 1.0. Compared to amines, amides are weaker bases, and therefore do not present noticeable acid–base properties in water;[61] they are protonated only at a low pH (<4). In the solution of the metal and peptide at a 1 : 3 molar ratio, at pH 4.0, two additional bands appear, with maximum values at 491 and 457 nm; these bands can be attributed to the $[Fe(\mathbf{P1})_2H_2]^{3+}$ and $[Fe(\mathbf{P1})_3H_3]^{3+}$ complexes, respectively. The positive charge of the $[Fe(\mathbf{P1})_2H_2]^{+}$ complex is associated with the metal ion and the protonated amine on the N-end of the peptides. The ESI-MS spectra (Fig. S9†) recorded in 50/50 H_2O/MeCN solution showed the formation of the $[Fe(\mathbf{P1})H_{-1}]^{+}$ ($[C_{26}H_{34}FeN_6O_8]^{+}$; Fig. S9a†) and $[Fe(\mathbf{P1})_2]^{+}$ ($[C_{52}H_{70}FeN_{12}O_{16}]$; Fig. S9b†) complexes.

The **P2** peptide is considered a $[LH_4]^{2+}$ ligand with amine, amide, hydroxyl and carboxylic dissociating groups. Fig. 3A shows the absorptivity spectrum of the **P2** complex with iron(III) ions, at pH 4.6. The large band centered at 475 nm is composed of two bands (457 and 491 nm) of almost the same intensity, and one band at 540 nm of a lower intensity that represents the formation of all three types of complexes: $[Fe(\mathbf{P2})H]^{2+}$, $[Fe(\mathbf{P2})_2H_2]^{+}$ and $[Fe(\mathbf{P2})_3]$.

The similarities between the UV-Vis spectra of the 1 : 3 (metal : ligand) stoichiometry, **P1**- and **P2**-peptide complexes (Fig. 3A) and that of **DFP** (Fig. 1A) suggest that only **MIM** residues are involved in the coordination of the iron, whereas carboxylic groups are not part of the metal coordination core. Indeed, the DFT optimized complexes in solution show that carboxylic acid groups are not involved in the coordination of the iron, and that the metal ions are bound by the oxygen atoms of **MIM** residues (Fig. 4). For each one-mimosine peptide, we optimized the most likely 1 : 1 metal–ligand geometry and calculated its binding energy (Table 2); even though in Table 2 we also reported the binding energies of 1 : 1, 1 : 2 and 1 : 3 metal–**DFP** complexes, it is important to bear in mind that a direct comparison of the stability of these compounds with mimosine-containing peptides is not reliable. Indeed, it is not correct to compare the stability of bidentate ligands (DPF complexes) with those of hexadentate ligands (**MIM**-peptides) because of different entropic contributions related to their respective chelate effects.

A comparison of the free energies of the 1 : 1 complexes (Table 2) shows that Peptide 3 (**P3**) forms the most stable complexes with either copper and iron when compared with Peptide 1 and Peptide 2.

The reason for this higher stability could be due to the intra-molecular H-bonds that are formed between the coordinating water molecules and backbone carbonyl and carboxylate residues of **P3** (Fig. 4F and G); these interactions are supposed to stabilize the overall system when compared with **P1** and **P2**, although a thorough conformational analysis of all peptides is beyond the scope of the present work.

Likewise, the 1 : 1 Fe(III)–**P2** complex is more stable (ΔG_{aq} = −76.4 kcal mol^{-1}) than the complex formed with **P1** (ΔG_{aq} = −65.4 kcal mol^{-1}), whereas the 1 : 1 Cu(II)–**P2** and Cu(II)–**P1** complexes have similar stability. Again, in the case of the Fe(II)–**P2** complex (Fig. 4C), intra-molecular hydrogen bonds are

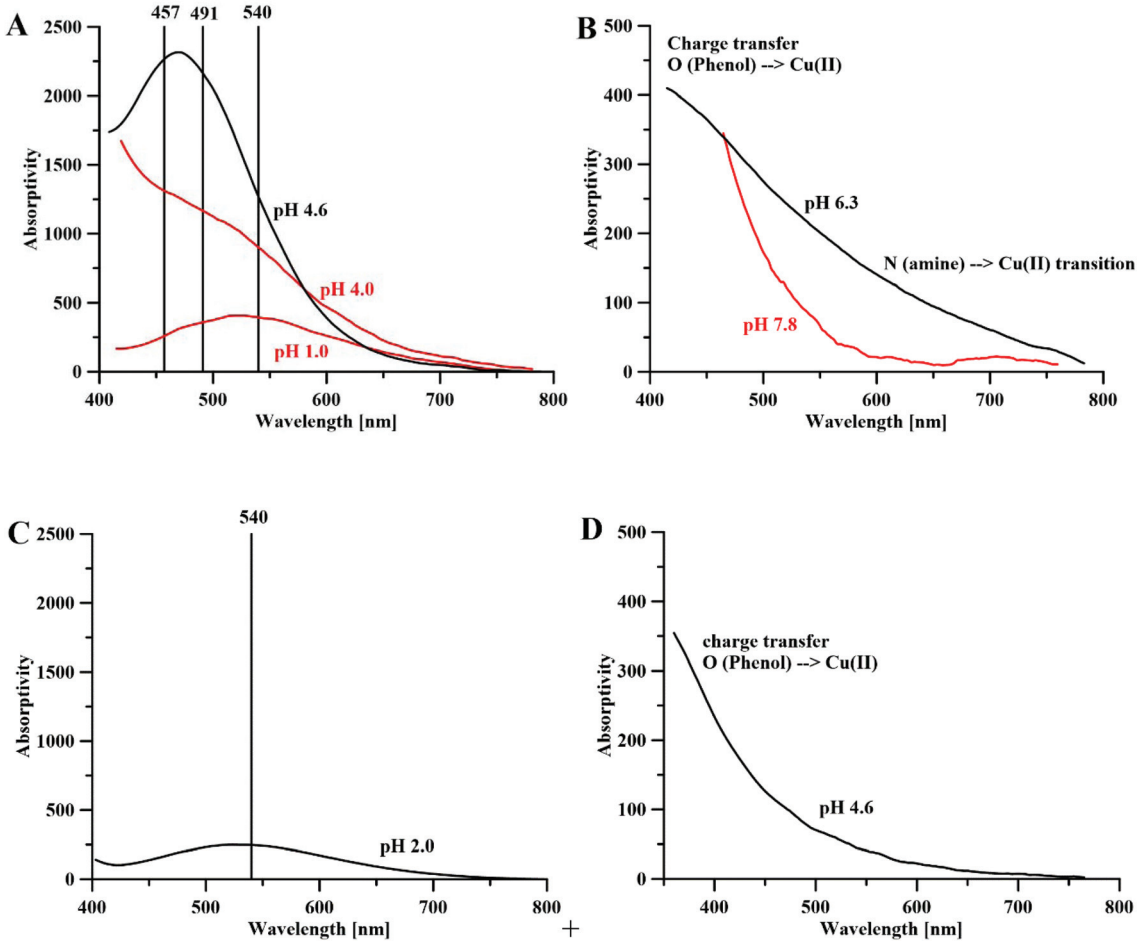

Fig. 3 Absorptivity spectra of (A) Fe^{3+}–**P1** (red) and Fe^{3+}–**P2** complexes (black), metal : ligand molar ratios 1 : 1 and 1 : 3 (for **P1**) and the ratio 1 : 3 (for **P2**), [**P1**] = [**P2**] 10 mM, *l* = 0.13 cm; (B) the Cu^{2+}–**P1** (red) and Cu^{2+}–**P2** (black) complexes, the metal : ligand molar ratio 1 : 2, [**P1**]=[**P2**] = 10 mM, *l* = 0.13 cm. (C) Fe^{3+}–**P4** complexes, the metal : peptide molar ratio 1 : 1, [**P4**] = 30 mM, *l* = 0.13 cm and (D) Cu^{2+}–**P4** complexes, the metal : peptide molar ratio 1 : 1, and [**P4**] = 30 mM and *l* = 0.13 cm.

additional forces that concur in the higher stabilization of the system.

For the same reasons outlined above, the 1 : 1 Fe(III)–**P3** and Cu(II)–**P3** complexes are remarkably more stable than the respective 1 : 1 metal–**DFP** complexes (Table 2).

The Vis spectra of the Cu^{2+}–**P1** complexes are shown in Fig. 3B. At a slightly basic pH, only the high intensity charge transfer O(phenol) → Cu^{2+} band appears to occur, which suggests the formation of a $[Cu(\mathbf{P1})_2H_2]^{2+}$ complex. The absence of the bands in the 600–800 nm range implies that neither the amine group (N-end and C-end of the peptide) in the metal coordination shell nor the free metal ion in the solution is present. The ESI-MS spectra (in 50/50 H_2O/MeCN solution; Fig. S10†) showed the presence of the $[Cu(\mathbf{P1})H_{-1}]^+$ ($[C_{26}H_{34}CuN_6O_8]^+$) complex (Fig. S10a†).

The **P2** complexes with copper(II) ions, at pH 6.3, are different from those of **P1** (Fig. 3B). Next to the band of charge transfer O(Phenol) → Cu^{2+}, we notice the presence of the d–d transition band (~650 nm) N(amine) → Cu^{2+} transition, which confirms the implication of the nitrogen atoms in the metal coordination shell. The high intensity of the absorptivity spectrum (in agreement with the literature Cu(II)–mimosine complex data[59] in Table 1) suggests the formation of the dinuclear complex $[Cu_2(\mathbf{P2})_2]$ (Fig. 4E), where each copper(II) ion is coordinated by the mimosine (CO, O^-) and aspartic acid (NH_2, COO^-) residues.

The copper(II) 1 : 1 stoichiometry complexes of **P1**, **P2** and **P3**, characterized by DFT calculations (Fig. 4A–D, F and G), confirm that the Cu(II) ion is coordinated by the pair of hydroxyl and carbonyl atoms of the **MIM** residue and three water molecules.

Considering the stability of the $Cu_2(\mathbf{P2})_2$ complex, it is evident that unlike the dinuclear copper(II)–**MIM** complex where Cu(II) ions appear penta-coordinated, in the $Cu_2(\mathbf{P2})_2$ system the two Cu(II) ions are tetra-coordinated by interacting with the **MIM** moiety of one peptide and the terminal carboxylic and amino groups of the other peptide (Fig. 4E). However, the interaction of Asp1 amino acid through its side chain carboxylic group and terminal amine slightly distorts the planarity between the metal ligands (Table S10†).

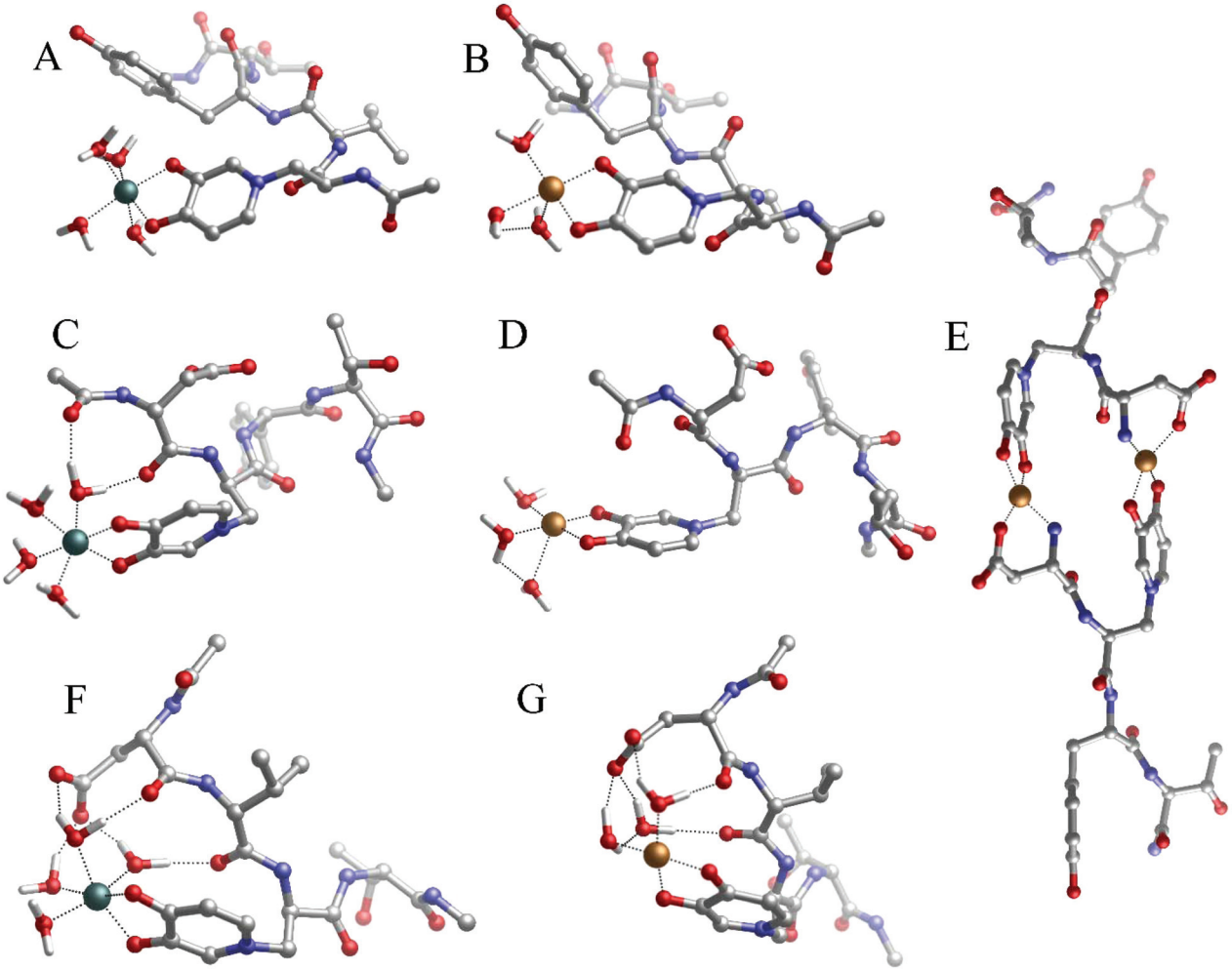

Fig. 4 Geometries of (A) Fe(**P1**), (B) Cu(**P1**), (C) Fe(**P2**), (D) Cu(**P2**), (E) Cu_2(**P2**)$_2$, (F) Fe(**P3**) and (G) Cu(**P3**) complexes optimized with DFT in solution.

Nevertheless, the metal coordination shell of the **P2** dinuclear complex is similar to that of the 2 : 2 copper(II)–**MIM** complex, with the Cu(II)–ligand binding site distances and angles being nearly the same (Table S10†). The stabilities of such complexes were computed according to eqn (3).

Cu(II) is tetra-coordinated both in solution and within the complex. The computed free energy value of the tetra-coordinated Cu_2(**P2**)$_2$ (−178.2 kcal mol^{-1}) complex is considerably more stable than the penta-coordinated Cu_2(**MIM**)$_2$ (−163.1 kcal mol^{-1}) one.

3.1.3. Two-mimosine peptides: Peptide 4 (H-Mim-Gly-Mim-Gly-OH) and Peptide 5 (H-Mim-Gly-Pro-Gly-Mim-Gly-OH). Peptide 4 has two **MIM** residues, spaced with glycine residues. The $[LH_4]^+$ ligand has four dissociating groups: amine (N-end), carboxylic (C-end) and two hydroxyl groups of **MIM** residues. Contrary to peptides **P1** and **P2**, peptide 4 contains two **MIM** residues, and, for this reason, the UV-Vis studies of iron(III) and copper(II) complexes are performed in solutions with a 1 : 1 metal-to-peptide molar ratio. Fig. 3C presents the

Table 2 Binding enthalpies (ΔH_{aq}) and free energies (ΔG_{aq}) in solution (in kcal mol^{-1}), computed according to eqn (2) on the DFT complexes formed by the six peptides given in Table 1, and by Fe(III) or Cu(II). For the sake of comparison, the energies of the copper(II) and iron(III) complexes in different molar ratios are also shown

Ligand name	Metal : ligand stoichiometry	Fe(III)		Cu(II)	
		ΔH_{aq}	ΔG_{aq}	ΔH_{aq}	ΔG_{aq}
DFP	1 : 3	−159.7	−165.3	—	—
DFP	1 : 2	−124.6	−131.2	−92.5	−97.6
DFP	1 : 1	−78.3	−81.5	−53.5	−56.1
Pept1	1 : 1	−70.2	−65.4	−51.8	−53.9
Pept2	1 : 1	−79.2	−76.4	−47.7	−50.9
Pept2	2 : 2			−159.7	−178.2
Pept3	1 : 1	−100.2	−91.4	−76.3	−69.5
Pept4	1 : 1	−109.7	−123.0	−74.3	−79.9
Pept4	2 : 2			−170.8	−187.0
Pept5	1 : 1	−106.7	−119.1	−65.3	−73.9
Pept5	2 : 2			−197.1	−205.9
Pept6	1 : 1	−121.9	−152.9	−60.9	−88.2

absorptivity spectrum of the iron(III) ions with the **P4** peptide, at pH 2.0. The single band with the maximum absorptivity at 540 nm suggests the formation of a monomeric $[Fe(\mathbf{P4})H_3]^{3+}$ species, positively charged due to its iron ion and amine group, whereas the second hydroxyl group and the carboxylic groups remain protonated at this low pH. It is unlikely that a dimeric complex is formed at such very low pH.

DFT calculations in water show the formation of a monomeric species Fe(III)/**P4** (Fig. 5A), where **MIM** residues are close enough to form a cyclic complex, and where two **MIM** and two water molecules form a complex exhibiting octahedral geometry (Table S11† and Fig. 5A).

Fig. 3D shows the absorptivity spectrum of the Cu(II)–**P4** system, in which only the band of charge transfer O(Phenol) → Cu^{2+} is present. This implies the existence of a coordination of the copper(II) by 2 (CO, O–) pairs of oxygen atoms of two **MIM** residues (Fig. 5B). The spacer between the two **MIM** residues is too short to allow both **MIM** residues participate in the coordination of the copper ion (Fig. 5B) and, due to the steric encumbrance, it is more likely that a dinuclear complex $[Cu_2(\mathbf{P4})_2]$ (Fig. 5C) is formed, instead of a monomeric species [Cu(**P4**)]. The formation of a dimeric complex, in which each metal ion is coordinated by two **MIM** residues (Fig. 5C), is consistent with the absorptivity spectrum of the Cu(II)/**P4** system obtained in our study (Fig. 3D).

Peptide 5 contains two **MIM** residues spaced by three amino acid residues. It has the same dissociating groups as peptide 4, and is considered to be a $[LH_4]^+$ ligand, but it is longer than **P4** due to the presence of additional glycine and proline residue. The proline residue was introduced in the middle of the peptide's backbone to support turn formation upon metal complexation.[1]

DFT calculations highlight that the 1 : 1 iron to **P5** complex has two **MIM** residues and two water molecules in the metal-coordination core (Fig. 5D). The Fe(III) coordination shells are very similar, with both **P4** and **P5** systems satisfying the optimal octahedral coordination mode of iron (geometric data are given in Table S11†). Therefore the slightly lower stability of Fe(III)–**P5** compared to the Fe(III)–**P4** complex (Table 2) could be due to the rigidity of the peptide backbone that contains the proline residue; however, we reiterate that a careful conformational analysis (beyond the scope of this work) is pivotal in order to examine this point.

According to DFT calculations, **P5** can form a monomeric Cu(II)–**P5** complex in which two **MIM** residues and two water molecules coordinate copper ions in the distorted octahedral complex (Fig. 5E). Also in this case, the stability of the monomeric Cu(II)–**P5** complex is lower than that of the monomeric Cu(II)–**P4** system (Table 2) and, analogously to **P4**, it is highly possible that copper dimeric species (Fig. 5F) are formed. Finally, a comparison of the stabilities of the **P5** and **P4** dimeric complexes with the copper(II) ion reveals that the former is remarkably more stable than the latter.

3.1.4. Three mimosine peptide: Peptide 6 (H-Mim-Gly-Pro-Gly-Mim-Gly-Gly-Mim-OH). Peptide 6 has three mimosine residues spaced by glycine and one proline. It is a $[LH_5]^+$ ligand with three dissociating hydroxyl groups of **MIM** residues, one amine group at the N-end, and one carboxylic group at the C-end of the peptide.

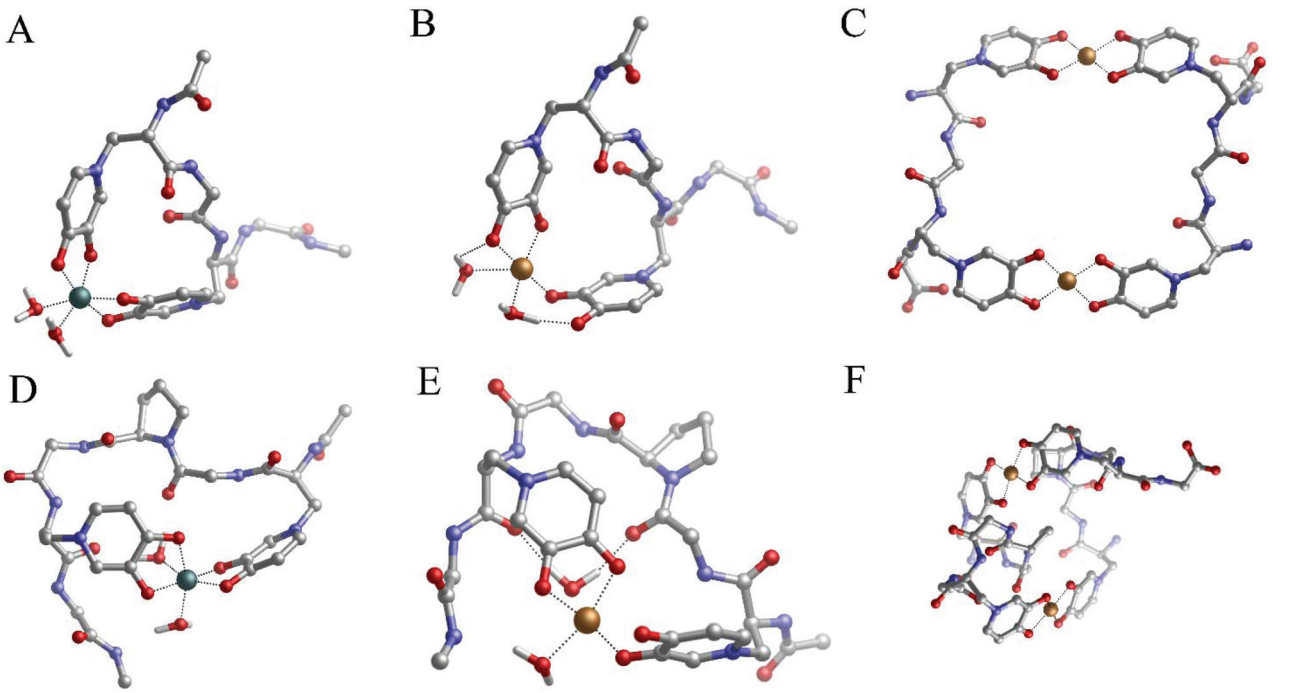

Fig. 5 Geometries of (A) the Fe(III)/**P4** 1 : 1 complex, (B) the Cu(II)–**P4** 1 : 1 complex, (C) the Cu(II)–**P4** 2 : 2 complex, (D) the Fe(III)–**P5** 1 : 1 complex, (E) the Cu(II)–**P5** 1 : 1 complex and (F) the Cu(II)–**P5** 2 : 2 complex optimized with DFT in solution.

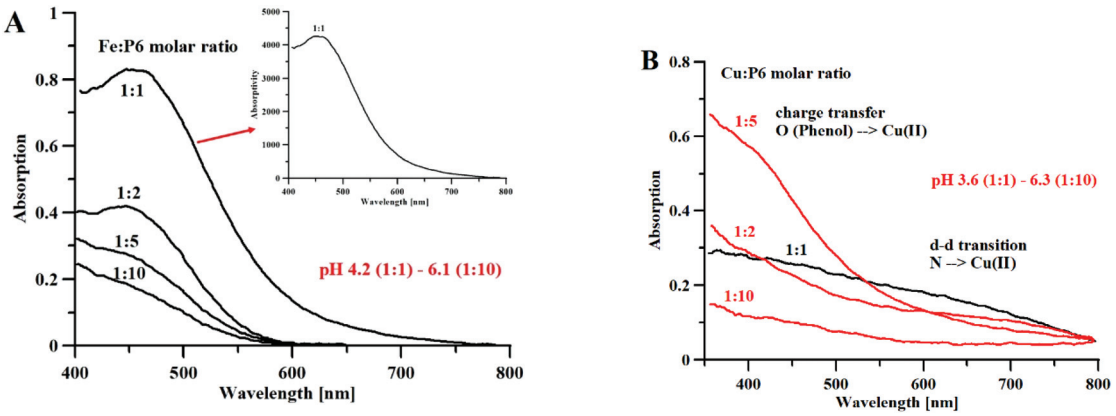

Fig. 6 (A) Absorption and absorptivity spectra of Fe^{3+}–**P6** complexes, [**P6**] = 1.5 mM, l = 0.13 cm (B) Absorption spectra of Cu^{2+}–**P6** complexes, [**P6**] = 3.5 mM, l = 1.0 cm.

Fig. 6A shows the Vis spectra of the iron(III)–**P6** system titration with the growing quantity of iron ions. We can clearly see that the spectrum reaches its highest absorptivity for a 1 : 1 metal to peptide molar ratio, which is equivalent to the maximum absorptivity of the Fe(**DFP**)$_3$ complex (Fig. 1A). Based on this result, we can hypothesize the formation of a monomeric Fe(**P6**) complex, where the metal ion is coordinated by six oxygen atoms of three mimosine residues (Fig. 7A).

Fig. 6B shows the results of an analog experiment with copper(II) ions. At a high metal-to-ligand molar ratio (1 : 10), and a pH of 6.3, only the band of charge transfer O(Phenol) → Cu^{2+} can be observed. In the solutions of 1 : 5 and 1 : 2 metal to ligand molar ratios, the band of charge transfer is predominant (over the band of the N(amine) → Cu^{2+} d–d transition). In the solution containing equimolar concentrations of metal and peptide, at pH 3.6, the intensity of the charge transfer band is almost equal to the band of the d–d transition, which makes it likely that mixed coordination complexes are formed.

The 1 : 1 complexes formed by peptide 6 and Fe(III) or Cu(II) were characterized by DFT methods and their binding energies computed, according to eqn (2). For both complexes, the optimized structures are shown in Fig. 7A and B respectively, and their computed binding energies in solution are presented in Table 2.

The spacers between the mimosine residues are long enough to involve three mimosine residues in the metal-coordination process. In fact, the angles computed on the metal coordination shell of Fe(**P6**) are very similar to the ones computed on Fe(**DFP**)$_3$ (see Table S11†), indicating that the peptide is long enough to allow the three mimosine side chain to arrange in a near-optimum disposition. Interestingly, the free energy (Table 2) of the Fe(III)–**P6** complex (−152.9 kcal mol^{-1}) is less negative compared to that of the 1 : 3 Fe(III)–**DFP** (−165.3 kcal mol^{-1}) and very similar to that of the 1 : 3 Fe(III)–**MIM** complex (−151.8 kcal mol^{-1}, Table S2†). Such a situation indicates that, in the case of **P6**, the entropic contribution related to the chelate effect is not a major driving force in the stabilization of 1 : 1 Fe(III)–**P6**, as highlighted by the very similar free energy of the 1 : 3 Fe(III)–**MIM** complex. A possible explanation could be that the introduction of one proline residue turns the backbone of the peptide, but makes it more rigid and decreases its overall complex stability. Clearly, the addition of a proline residue is not a good strategy for the design of novel mimosine-containing chelating agents with

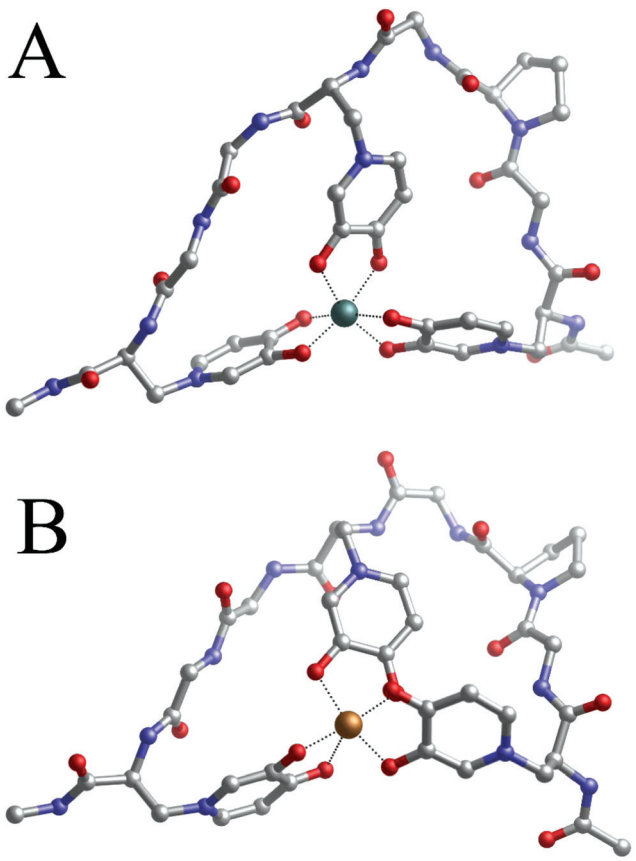

Fig. 7 Geometries of Fe(III)–**P6** (A) and the Cu(II) (B)–**P6** 1 : 1 complex optimized with DFT in solution.

improved chelation performance. These findings are in agreement with the results obtained in our previous work involving proline-containing and proline-free mimosine peptides coordinating Al(III) ions.[42]

Regarding the Cu/**P6** monomeric complex, apparently the metal adopts octahedral coordination mode because the angles between the oxygen ligands are appropriate for this coordination mode (see Table S12†). However, one of the mimosine residues interacts only though one oxygen atom (Cu–O distances of 1.98 and 2.80 Å), and a second one is in the mono-/bidentate borderline (Cu–O distances of 1.97 and 2.41 Å). Even if two **MIM** residues are involved in the coordination of copper, the geometry of the complex is distorted, and two of the **MIM** residues are not in planar position, with respect to the central metal ion. It is evident that the length of the linker between the neighboring metal binding **MIM** residues is too short to allow the formation of a complex of octahedral geometry, similar to that of Cu(**DFP**)$_2$, where two ligand molecules are in planar and equatorial positions. It is more likely that stoichiometries different than 1 : 1 are formed with the co-participation of the amine group in the complex core, as it can be deduced from Vis spectra with the evident N(amine) → Cu^{2+} d–d transition band (Fig. 6B).

Theoretical TDDFT spectra of metal complexes with **DFP** and all studied peptides confirmed our analysis of the UV/Vis experimental spectra and showed good agreement with the experiments. For a complete analysis of the theoretical spectra, we refer to the ESI (Fig. S11–S15†).

3.1.5. Improving the metal binding affinity: the role of the methyl group. Looking at Scheme 1, a clear difference between the **DFP** and **MIM** ligands indicates the presence of a methyl group in the ring of the former, but not of the latter. In order to assess the effect of the CH_3 substituent towards the stability of the Fe(III) and Cu(II) complexes with deferiprone (**DFP**) and mimosine (**MIM**) ligands, we calculated DFT models of the complexes formed by Fe(III) and Cu(II) with **DFP**- and mimosine-based complexes, using our previously validated computational protocol.[52] We also compared the experimental stability constants from our study with those reported in the literature (Table S2 and Fig. S8†). Finally, we characterized two model compounds, one with and one without the –CH_3 substituent placed in the ring, for both **DFP** and **MIM** ligands, providing a total of four different ligands (**DFP**, **DFP-unmet**, **MIM**, and **MIM-unmet**; Scheme 1). It is worth noting that the methyl group is an electron-donating (ED) substituent through inductive effect that is expected to increase the ligand's affinity towards trivalent metals, due to a slight increase in the (minor) covalent character of the metal–ligand dative interactions.[52]

As seen in Fig. S8,† the binding energies computed in solution (ΔG_{comp}, see Table S2†) are in very good agreement with the available $\log\beta$ values with a correlation coefficient of 0.9873, confirming the suitability of our methodology for the characterization of the complexes investigated in this study. Interestingly, the **DFP** ligand interacts more tightly with the two metals than it does with the **MIM** residue; with Fe(III) and the 1 : 1, 1 : 2 and 1 : 3 complexes containing **DFP** being, respectively, 9.2, 15.4 and 15.6 kcal mol^{-1} more stable than the **MIM**-containing ligands. In the case of Cu(II), the 1 : 1 and 1 : 2 ligands that contain **DFP** are, respectively, 6.1 and 13.2 kcal mol^{-1} more stable than their **MIM**-containing counterparts.

Considering both families of ligands (deferiprone-based and mimosine-based), the introduction of a methyl group significantly increases the stability of the formed complexes, especially the stability of the iron complexes (Table S2†). For Fe(III), for example, the Fe–**DFP** 1 : 1, 1 : 2 and 1 : 3 complexes are 4.3, 8.0 and 7.0 kcal mol^{-1} more stable than the corresponding Fe–**DFP-unmet** (Table S2†). Similarly, in the case of Cu(II), the presence of methyl in the Cu(II)–**DFP** complexes also leads to more stable complexes than the Cu(II)–**DFP-unmet** complexes (2.7 and 3.5 kcal mol^{-1} for the 1 : 1 and 1 : 2 complexes). However, the increase in stability, upon addition of the methyl group, is lower than that obtained with the Fe(III)–ligand complexes. Interestingly, a similar trend is also observed for the **MIM**-based ligands, for which the inclusion of the –CH_3 substituent stabilizes all complexes in a similar fashion. The addition of a methyl in position 2 in the mimosine ligand (**MIM-met**) stabilizes the Fe(III) 1 : 1, 1 : 2 and 1 : 3 complexes by 4.5, 7.5 and 4.9 kcal mol^{-1}, respectively; the Cu(II) 1 : 1 and 1 : 2 complexes are stabilized by 2.4 and 6.5 kcal mol^{-1}, respectively.

In general, we can conclude that the addition of a 2-methyl group is important for augmenting the affinity of **DFP** to the metal, but the introduction of the 3-methyl substituent in mimosine would lead to a lower increase in affinity. This is probably due to the positively charged amino group of the **MIM** residue, which acts as an electron-withdrawing group (EW), thus lowering the electron density from the coordination site of the ligands. As a result, the EW amino group (positively charged) partially compensates the ED effect of the methyl group. Nevertheless, the addition of this 2-methyl group could help in the improvement of the chelation performance of these compounds.

3.2. Antimicrobial activity

Antimicrobial peptides (AMPs) (also known as host defence peptides, HDPs) are part of the innate immune response, in all classes of life, produced to kill bacteria, viruses, fungi and even cancer cells.[62–65] Most AMPs have a positive charge (+2 to +9) and hydrophobic amino acids (more than 30%), while the length varies between 10 and 50 amino acid residues. The mechanism of AMP action against microbials is complicated and the same AMP may act on different targets.[63] One of the best known mechanisms is through membrane permeabilization, which consequently leads to a loss of cellular components and cell death.[64] The non-specific membrane interactions between AMPs and bacteria differ from those of antibiotics, and they target specific molecular receptors of pathogens and make it difficult for bacteria to acquire resistance to AMPs.[64]

Different approaches have been used to ameliorate AMP bactericidal activity with a short half-time and at the same

time reduce hemolytic activity, *e.g.* changes in the amino acids' sequence, cyclization, and synthesis of multivalent constructs. It was observed that the proline-rich peptides have a higher membrane internalization, while Gly-rich peptides are more selective for Gram-negative bacteria, fungi and cancer cells.[65,66] Also many short-chain pro-rich peptides showed a high activity against Gram-negative bacteria.[67] The long peptides with a high ratio of Pro and Gly amino acids usually exhibit linear, rather than secondary, structures.[68–70] AMPs have mostly a positive charge (from +2 to +9), which allows AMPs to interact with negatively charged lipid head groups.[71] The increase of the positively charged amino acids in the peptides' sequence increases the affinity for the microbial membrane and improves the overall antimicrobial activity. However, also anionic AMPs (containing Gln and Asp) participate in the eukaryotic innate immune system.[72] Their negative charge ranges from −1 to −2, and they generally need cations (*e.g.* Zn^{2+}) as cofactors for antibiotic activity.[73]

AMPs with high hydrophobicity can damage the membrane structure, which results in cell lysis or the formation of transient pores and the transport of peptides inside the cell; this property enables them to interact with intracellular targets.[74]

3.2.1. Antibacterial and antidermatophytic activity. Mimosine peptides are stable in solid state and in water solution for weeks. No experimental changes were observed in repeated NMR spectra nor in microbiological studies conducted over three months. The high stability could be associated with the non-protein mimosine amino acid, which is not recognized by the proteolytic enzymes.

The preliminary screening carried out on the six peptides by the disk diffusion method (Table S14†) reveals that the peptides tested at higher concentrations possess an antibacterial activity. In particular, **P5** (810 μg per disk equivalent to 81 mg mL^{-1}) exhibits an inhibitory effect against *S. aureus* and *B. cereus*, and **P3** (340 μg per disk) against *S. aureus*. The other four peptides tested with lower concentrations show no inhibition activity against the microbial strains used as indicators.

The physicochemical properties of the peptide, with respect to charge, amphipathic nature, hydrophobicity capacity, are key factors impacting on their mode of action and selectivity towards microbial cells.[75] The binding of the metal may induce changes to net charge and the conformational plasticity of the peptides that may favor the interaction with the bacterial cell wall and the phospholipid bilayer component of the membrane, resulting in the potentiation of antibacterial activity; however, additional experiments need to be performed to confirm such hypothesis.

In order to better investigate the antibacterial activity of the mimosine-derived peptides and their complexes, the MIC and MBC values were determined following the broth microdilution method. The results are reported in Tables S15 and S16.† The copper complexes with the peptides investigated in our study showed no antibacterial activity, whereas the iron(III) complexes with the **P4** and **P6** peptides gave a positive antibacterial response. The free **P4** shows an MIC of 7450 μg mL^{-1}, and the iron(III) complex of **P4** shows up to fifteen times lower MIC values against *S. aureus* (484 μg mL^{-1}), *B. cereus* (484 μg mL^{-1}), and *E. coli* (967 μg mL^{-1}). A good inhibition activity was recorded against the strains *S. aureus* and *B. cereus* by the **P6** Fe complex, with MIC values of 448 μg mL^{-1}, which are much lower than the MIC activity of the free **P6** peptide (>6900 μg ml^{-1}).

The enhanced antagonistic activity of the iron complexes against *Bacillus* could be due to the siderophore mimicking property of the mimosine peptides, these being structurally similar to the siderophores produced by *Bacillus* strains (*e.g.* petrobactin), but more in-depth studies aimed at understanding the mechanism of action are needed for supporting this hypothesis. The siderophore mimicking property of mimosine peptides could be applied for diagnostic and theragnostic treatment of bacterial infections,[76] while mimosine is structurally similar to that of **DFP** and could form stable complexes with Gd(III)[77] and other lanthanide metals.[37]

Mimosine based peptides are structurally and functionally different from classical antibiotics and their MIC activity should be compared with AMPs rather than antibiotics. The MIC comparative studies of different AMPs made by Ebbensgaard *et al.*[5] showed that unstructured AMPs (Myxinidin-NH2, Pyrrhocoricin, Apidaecin IA, Metalnikowin I) are less effective than α-helical and β-sheet structured peptides and their MIC activity requires more than 256 μg mL^{-1} concentration. Such a value is comparable with the results reported for the Fe(III)–**P6** complexes.

Even if mimosine peptides require high doses to reach MIC activity, their month-long stability, both in the solid state and in solution, makes them good candidates for being an alternative to antibiotics (or mixed) therapies. Recent studies point out that the contemporary use of different antibiotic agents can reduce the dose of each drug in the combination. Such mixed therapies may lower the development of bacterial resistance *in vitro* (compared to monotherapy). AMPs/peptidomimetics are well suited for synergic combinations with conventional antibiotics,[64] while disrupting bacterial membranes and facilitating antibiotics to reach their cytosolic targets.[78]

3.2.2. Antibiofilm activity. Biofilm-associated-bacteria are responsible for up to 65% of infections in humans and at the same time are highly adaptively resistant to classical antibiotics. Biofilm forms on living tissues, medical devices, industrial or potable water system piping, or in the natural aquatic environment.[79] Almost 80% of human infections are caused by biofilms.[80–82] Biofilm infection can be classified into two groups, non-device and device associated infections.[83,84] About 60–70% of nosocomial infections are related to biomaterials or implants.[85] It is difficult to remove biofilm formation on medical devices, therefore necessitating the removal of the infected device or use of high doses of antibiotics,[86] which increases costs and further antibiotic resistance and cytotoxicity.[87] Therefore, the identification of new compounds (*e.g.* peptides) capable of inhibiting biofilm formation is required.

Natural and synthetic antimicrobial peptides have been shown to prevent biofilm formation, kill bacteria or disrupt

the biofilm structure.[88] AMPs prevent bacteria adhesion on surfaces[89] and damage mature biofilms by detachment or killing bacteria.[90] The exact mechanism of biofilm degradation is poorly understood, but the fast destruction of biofilm embedded cells[90] may indicate that they act by disrupting the membranes of the bacteria.

In this study the antibiofilm activity of the most effective inhibitor (peptide 6) and its Fe complex is evaluated. Three different strains of bacterial pathogens (*S. aureus*, *S. intermedius*, and *P. aeruginosa*), described in the literature as linked to biofilm-associated diseases in humans and animals,[91,92] are used to examine the antibiofilm activity of peptide 6 and its iron complex. A preliminary evaluation of **P6** against bacteria in Planktonic status shows (Table S17†) an antimicrobial activity (MIC > 1 mM L^{-1}; MBC > 1 mM L^{-1}), whereas **P6** in sessile form shows a slightly different behavior. Peptide 6 is found unable to completely inhibit the formation of biofilms, but a consistent reduction (up to 70%) related to the peptide's concentration is observed for *S. aureus* (from 1 to 0.5 mM peptide concentration range). The antibiofilm data show that the **P6** Biofilm–interaction is not iron-dependent (P > 0.05 between two conditions +Fe/−Fe), as seen in Fig. S7A,† suggesting that **P6** activity against biofilm formation is rather not related to siderophore mimicking. With respect to the other bacterial strains, *S. intermedius* and *P. aeruginosa*, the obtained values, at different peptide concentrations, with and without iron, are not significant; nevertheless, the addition of iron ions to the peptide solution slightly reduces the formation of a biofilm (Fig. S7B and C†). The antibiofilm results reported here are preliminary, and should be more thoroughly examined by the genic expression of biofilm-related genes, for example those involved in the bacteria quorum-sensing network.[92]

The anti-biofilm activity of AMPs can be enhanced by mixed therapy with antibiotics.[93–95] Combine use of AMPs with known antibiotics is useful since they can target different strains of bacteria with different metabolisms cells in low pH, hypoxic or low nutritious environments.[96]

4. Conclusions

We have presented a series of mimosine-based peptides, which according to our experimental and theoretical data, are effective iron(III) and copper(II) chelators. These peptides bind Fe(III) more strongly than Cu(II), as non-peptidic complexes based on deferiprone. Quite interestingly, the binding energies of these peptide complexes can be modulated by a number of key structural factors, such as the number of mimosine residues in the peptide, and length and flexibility of the spacer between mimosine residues. In this sense, peptide 6, with three mimosine residues, forms the most stable complexes with both Fe(III) and Cu(II), followed by peptides 4 and 5, with two mimosine residues.

For each peptide, the basic metal : peptide stoichiometry was investigated. The formation of oligomeric and polymeric structures depends on environmental factors (peptide and metal concentration, pH, ionic strength and temperature) and needs further investigation in diffusion NMR studies. The present results and the combination of theoretical and experimental methodologies can be helpful for the design of self-assembly between metal ions and mimosine peptides, which could lead to various medical and nanotechnological applications. In fact, we have also proved that Fe–mimosine complexes can display a significant antimicrobial activity, which highlights the potential interest of the compounds presented in this work.

Conflicts of interest

There are no conflicts to declare.

Acknowledgements

This work was supported by a grant no. UMO-2015/17/D/ST5/01329 from the National Science Centre, Poland. This work was also supported by Grants PGC2018-099321-B-I00 from the Ministry of Science and Universities through the Office of Science Research (MINECO/FEDER), and Grant IT588-13 from the Basque Government.

References

1 R. Zou, Q. Wang, J. Wu, J. Wu, C. Schmuck and H. Tian, *Chem. Soc. Rev.*, 2015, **44**, 5200–5219.
2 D. E. Przybyla and J. Chmielewski, *Biochemistry*, 2010, **49**, 4411–4419.
3 M. Panciera, M. Amorín and J. R. Granja, *Chem. – Eur. J.*, 2014, **20**, 10260–10265.
4 A. Ambrogelly, S. Palioura and D. Söll, *Nat. Chem. Biol.*, 2007, **3**, 29–35.
5 A. Ebbensgaard, H. Mordhorst, M. T. Overgaard, C. G. Nielsen, F. M. Aarestrup and E. B. Hansen, *PLoS One*, 2015, **10**, e0144611.
6 A. Lewies, L. H. Du Plessis and J. F. Wentzel, *Probiotics Antimicrob. Proteins*, 2019, **11**, 370–381.
7 K. Sabol, J. E. Patterson, J. S. Lewis, A. Owens, J. Cadena and J. H. Jorgensen, *Antimicrob. Agents Chemother.*, 2005, **49**, 1664–1665.
8 J. N. Steenbergen, J. Alder, G. M. Thorne and F. P. Tally, *J. Antimicrob. Chemother.*, 2005, **55**, 283–288.
9 S. Rotem and A. Mor, *Biochim. Biophys. Acta, Biomembr.*, 2009, **1788**, 1582–1592.
10 B. Findlay, G. G. Zhanel and F. Schweizer, *Antimicrob. Agents Chemother.*, 2010, **54**, 4049–4058.
11 N. Molchanova, P. Hansen and H. Franzyk, *Molecules*, 2017, **22**, 1430.
12 B. C. Q. Nguyen and S. Tawata, *Phytother. Res.*, 2016, **30**, 1230–1242.

13 S. Tawata, in *Pesticide and Alternatives*, ed. J.E Casida, Elsevier Science Publishers, Amsterdam, Netherlands, 1990, pp. 541–544.
14 J. W. Hylin, *Phytochemistry*, 1964, **3**, 161–164.
15 B. Tangendjaja, J. Hogan and R. Wills, *Aust. J. Agric. Res.*, 1983, **34**, 289–293.
16 R. Anitha, S. Jayavelu and K. Murugesan, *Phytother. Res.*, 2005, **19**, 992–993.
17 A. Zalatnai and J. Bocsi, *Anticancer Res.*, 2003, **23**, 4007–4009.
18 S. Frydas, N. Papaioannou, M. Papazahariadou, M. Hatzistilianou, E. Karagouni, M. Trakatelli, G. Brellou, C. Petrarca, M. Castellani and P. Conti, *Int. J. Immunopathol. Pharmacol.*, 2005, **18**, 85–93.
19 C. Baltazar, R. Mun, H. Tajmir-Riahi and J. Bariyanga, *J. Mol. Struct.*, 2018, **1161**, 273–278.
20 Y. Shan, Y. Ma, M. Wang and Y. Dong, *Curr. Med. Chem.*, 2012, **19**, 5885–5894.
21 Y. Dai, B. Gold, J. K. Vishwanatha and S. L. Rhode, *Virology*, 1994, **205**, 210–216.
22 T. Xuan, A. Elzaawely, F. Deba, M. Fukuta and S. Tawata, *Agron. Sustainable Dev.*, 2006, **26**, 89–97.
23 R. Williams and R. Hoagland, *Allelopathy J.*, 2007, **19**, 423–430.
24 M. Lalande, *Exp. Cell Res.*, 1990, **186**, 332–339.
25 A. Restivo, L. Brard, C. Granai and N. Swamy, *J. Clin. Oncol.*, 2005, **23**, 3200–3200.
26 K. Ward and R. N. Harris, *Aust. J. Biol. Sci.*, 1976, **29**, 189–196.
27 J. Savulescu, *Br. Med. J.*, 2004, **328**, 358.
28 FDA NEWS RELEASE: FDA Approves Ferripox (deferiprone) to Treat Patients with Excess Iron in the Body, Oct. 14, 2011, http://www.fda.gov/NewsEvents/Newsroom/PressAnnouncements/ucm275814.htm.
29 R. Ma, J. J. Reibenspies and A. E. Martell, *Inorg. Chim. Acta*, 1994, **223**, 21–29.
30 R. J. Motekaitis and A. E. Martell, *Inorg. Chim. Acta*, 1991, **183**, 71–80.
31 E. T. Clarke and A. E. Martell, *Inorg. Chim. Acta*, 1992, **191**, 57–63.
32 V. M. Nurchi, G. Crisponi, T. Pivetta, M. Donatoni and M. Remelli, *J. Inorg. Biochem.*, 2008, **102**, 684–692.
33 J. Lachowicz, V. Nurchi, G. Crisponi, M. Jaraquemada-Pelaez, M. Arca, A. Pintus, M. Santos, C. Quintanova, L. Gano and Z. Szewczuk, *Dalton Trans.*, 2016, **45**, 6517–6528.
34 E. T. Clarke, A. E. Martell and J. Reibenspies, *Inorg. Chim. Acta*, 1992, **196**, 177–183.
35 A. E. Gorden, J. Xu, K. N. Raymond and P. Durbin, *Chem. Rev.*, 2003, **103**, 4207–4282.
36 D. M. Doble, M. Melchior, B. O'Sullivan, C. Siering, J. Xu, V. C. Pierre and K. N. Raymond, *Inorg. Chem.*, 2003, **42**, 4930–4937.
37 K. H. Thompson, C. A. Barta and C. Orvig, *Chem. Soc. Rev.*, 2006, **35**, 545–556.
38 E. Chruscinska, E. Garribba, G. Micera and A. Panzanelli, *J. Inorg. Biochem.*, 1999, **75**, 225–232.
39 R. C. Scarrow, P. E. Riley, K. Abu-Dari, D. L. White and K. N. Raymond, *Inorg. Chem.*, 1985, **24**, 954–967.
40 A. Upadhyay, J. Chompoo, N. Taira, M. Fukuta, S. Gima and S. Tawata, *J. Agric. Food Chem.*, 2011, **59**, 12858–12863.
41 B. C. Q. Nguyen and S. Tawata, *Molecules*, 2015, **20**, 14334–14347.
42 J. Mujika, G. Dalla Torre, J. Lachowicz and X. Lopez, *RSC Adv.*, 2019, **9**, 7688–7697.
43 W. C. Chan and P. D. White, *Fmoc solid phase peptide synthesis*, Oxford University Press, 2000.
44 F. Delaglio, S. Grzesiek, G. W. Vuister, G. Zhu, J. Pfeifer and A. Bax, *J. Biomol. NMR*, 1995, **6**, 277–293.
45 T. Goddard and D. Kneller, *SPARKY 3.114*, University of California, San Francisco, USA, 2007.
46 K. Wüthrich, *Europhys. News*, 1986, **17**, 11–13.
47 A. D. Becke, *J. Chem. Phys.*, 1993, **98**, 5648–5652.
48 P. Stephens, F. Devlin, C. Chabalowski and M. J. Frisch, *J. Phys. Chem.*, 1994, **98**, 11623–11627.
49 S. Grimme, J. Antony, S. Ehrlich and H. Krieg, *J. Chem. Phys.*, 2010, **132**, 154104.
50 J. Tomasi, B. Mennucci and R. Cammi, *Chem. Rev.*, 2005, **105**, 2999–3094.
51 M. Frisch, G. Trucks, H. Schlegel, G. Scuseria, M. Robb, J. Cheeseman, G. Scalmani, V. Barone, G. Petersson and H. Nakatsuji, *Gaussian 16, Revision A*, 2016, vol. **3**.
52 G. Dalla Torre, J. I. Mujika, E. Formoso, E. Matito, M. J. Ramos and X. Lopez, *Dalton Trans.*, 2018, **47**, 9592–9607.
53 J. Alí-Torres, L. Rodríguez-Santiago and M. Sodupe, *Phys. Chem. Chem. Phys.*, 2011, **13**, 7852–7861.
54 B. Gandhi, R. Summerbell and T. Mazzulli, *J. Clin. Microbiol.*, 2018, **56**, e01481–e01417.
55 G. Orru, C. Demontis, A. Mameli, E. Tuveri, P. Coni, G. Pichiri, F. Coghe, A. Rosa, P. Rossi and G. D'Hallewin, *Front. Microbiol.*, 2017, **8**, 2067–2078.
56 W. Wang, S. Nema and D. Teagarden, *Int. J. Pharm.*, 2010, **390**, 89–99.
57 A. El-Jammal, P. L. Howell, M. A. Turner, N. Li and D. M. Templeton, *J. Med. Chem.*, 1994, **37**, 461–466.
58 W. C. Tsai and K. H. Ling, *J. Chin. Biochem. Soc.*, 1973, **2**, 70–86.
59 H. Stunzi, D. Perrin, T. Teitei and R. Harris, *Aust. J. Chem.*, 1979, **32**, 21–30.
60 R. P. Martin, L. Mosoni and B. Sarkar, *J. Biol. Chem.*, 1971, **246**, 5944–5951.
61 J. I. Lachowicz, M. Crespo-Alonso, F. Secci, C. Caltagirone, G. Alberti, R. Biesuz, J. O. Orton and V. M. Nurchi, *J. Trace Elem. Med. Biol.*, 2018, **50**, 580–588.
62 K. Reddy, R. Yedery and C. Aranha, *Int. J. Antimicrob. Agents*, 2004, **24**, 536–547.
63 K. A. Brogden, *Nat. Rev. Microbiol.*, 2005, **3**, 238–250.
64 J. Wang, X. Dou, J. Song, Y. Lyu, X. Zhu, L. Xu, W. Li and A. Shan, *Med. Res. Rev.*, 2019, **39**, 831–859.

65 E. de Souza Cândido, D. A. Sousa, J. C. Viana, N. G. de Oliveira-Júnior, V. Miranda and O. L. Franco, *Peptides*, 2014, **55**, 65–78.
66 N. Ilić, M. Novković, F. Guida, D. Xhindoli, M. Benincasa, A. Tossi and D. Juretić, *Biochim. Biophys. Acta, Biomembr.*, 2013, **1828**, 1004–1012.
67 W. Li, J. Tailhades, N. M. O'Brien-Simpson, F. Separovic, L. Otvos, M. A. Hossain and J. D. Wade, *Amino Acids*, 2014, **46**, 2287–2294.
68 E. Sikorska and E. Kamysz, *J. Pept. Sci.*, 2014, **20**, 952–957.
69 T. Niidome, H. Mihara, M. Oka, T. Hayashi, T. S. Kazutoshiyoshida and H. Aoyagi, *J. Pept. Res.*, 1998, **51**, 337–345.
70 E. J. Veldhuizen, V. A. Schneider, H. Agustiandari, A. Van Dijk, J. L. Tjeerdsma-van Bokhoven, F. J. Bikker and H. P. Haagsman, *PLoS One*, 2014, **9**, e95939.
71 X. Wang, J. C. B. Junior, B. Mishra, T. Lushnikova, R. M. Epand and G. Wang, *Biochim. Biophys. Acta, Biomembr.*, 2017, **1859**, 1350–1361.
72 N. B. Leite, L. C. Da Costa, D. dos Santos Alvares, M. P. dos Santos Cabrera, B. M. de Souza, M. S. Palma and J. R. Neto, *Amino Acids*, 2011, **40**, 91–100.
73 S. G. Dashper, N. M. O'Brien-Simpson, K. J. Cross, R. A. Paolini, B. Hoffmann, D. V. Catmull, M. Malkoski and E. C. Reynolds, *Antimicrob. Agents Chemother.*, 2005, **49**, 2322–2328.
74 A. Schmidtchen, M. Pasupuleti and M. Malmsten, *Adv. Colloid Interface Sci.*, 2014, **205**, 265–274.
75 N. Malanovic and K. Lohner, *Pharmaceuticals*, 2016, **9**, 59–92.
76 H. Kornreich-Leshem, C. Ziv, E. Gumienna-Kontecka, R. Arad-Yellin, Y. Chen, M. Elhabiri, A.-M. Albrecht-Gary, Y. Hadar and A. Shanzer, *J. Am. Chem. Soc.*, 2005, **127**, 1137–1145.
77 M. Rogosnitzky and S. Branch, *BioMetals*, 2016, **29**, 365–376.
78 R. Domalaon, T. Idowu, G. G. Zhanel and F. Schweizer, *Clin. Microbiol. Rev.*, 2018, **31**, e00077–e00017.
79 R. M. Donlan, *Emerging Infect. Dis.*, 2002, **8**, 881–890.
80 J. W. Costerton, P. S. Stewart and E. P. Greenberg, *Science*, 1999, **284**, 1318–1322.
81 L. Hall-Stoodley, J. W. Costerton and P. Stoodley, *Nat. Rev. Microbiol.*, 2004, **2**, 95–108.
82 F. Reffuveille, C. de la Fuente-Núñez, S. Mansour and R. E. Hancock, *Antimicrob. Agents Chemother.*, 2014, **58**, 5363–5371.
83 N. Høiby, T. Bjarnsholt, C. Moser, G. Bassi, T. Coenye, G. Donelli, L. Hall-Stoodley, V. Hola, C. Imbert and K. Kirketerp-Møller, *Clin. Microbiol. Infect.*, 2015, **21**, S1–S25.
84 U. Römling, S. Kjelleberg, S. Normark, L. Nyman, B. E. Uhlin and B. Åkerlund, *J. Intern. Med.*, 2014, **276**, 98–110.
85 J. D. Bryers, *Biotechnol. Bioeng.*, 2008, **100**, 1–18.
86 J. C. Carmen, B. L. Roeder, J. L. Nelson, R. L. R. Ogilvie, R. A. Robison, G. B. Schaalje and W. G. Pitt, *Am. J. Infect. Control*, 2005, **33**, 78–82.
87 I. K. Paterson, A. Hoyle, G. Ochoa, C. Baker-Austin and N. G. Taylor, *Sci. Rep.*, 2016, **6**, 37853–37863.
88 M. Yasir, M. Willcox and D. Dutta, *Materials*, 2018, **11**, 2468–2483.
89 G. Batoni, G. Maisetta and S. Esin, *Biochim. Biophys. Acta, Biomembr.*, 2016, **1858**, 1044–1060.
90 L. A. Segev-Zarko, R. Saar-Dover, V. Brumfeld, M. L. Mangoni and Y. Shai, *Biochem. J.*, 2015, **468**, 259–270.
91 L. Montanaro, A. Poggi, L. Visai, S. Ravaioli, D. Campoccia, P. Speziale and C. R. Arciola, *Int. J. Artif. Organs*, 2011, **34**, 824–831.
92 M. Erriu, C. Blus, S. Szmukler-Moncler, S. Buogo, R. Levi, G. Barbato, D. Madonnaripa, G. Denotti, V. Piras and G. Orrù, *Ultrason. Sonochem.*, 2014, **21**, 15–22.
93 N. M. Mishra, Y. Briers, C. Lamberigts, H. Steenackers, S. Robijns, B. Landuyt, J. Vanderleyden, L. Schoofs, R. Lavigne and W. Luyten, *Org. Biomol. Chem.*, 2015, **13**, 7477–7486.
94 H. Rudilla, E. Fusté, Y. Cajal, F. Rabanal, T. Vinuesa and M. Viñas, *Molecules*, 2016, **21**, 1223–1235.
95 S. M. Ribeiro, C. de la Fuente-Núñez, B. Baquir, C. Faria-Junior, O. L. Franco and R. E. Hancock, *Antimicrob. Agents Chemother.*, 2015, **59**, 3906–3912.
96 L. Grassi, G. Maisetta, S. Esin and G. Batoni, *Front. Microbiol.*, 2017, **8**, 2409–2417.